Available online at www.sciencedirect.com
ScienceDirect
Precambrian Research 162 (2008) 160–179
Precambrian Research
www.elsevier.com/locate/precamres

3.35 Ga komatiite volcanism in the western Dharwar craton, southern India: Constraints from Nd isotopes and whole-rock geochemistry

M. Jayananda [a,*], T. Kano [b], J.-J. Peucat [c], S. Channabasappa [a]

[a] Department of Geology, Bangalore University, Bangalore 560056, India
[b] Department of Earth Sciences, Yamaguchi University, Yamaguchi 753, Japan
[c] Géosciences-Rennes, Université Rennes 1, F-35042 Rennes, France

Received 12 July 2006; received in revised form 25 March 2007; accepted 4 July 2007

Abstract

We present field, petrographic, Sm–Nd whole-rock isochron and whole-rock geochemical data for komatiites from Sargur Group greenstone belts of the western Dharwar craton. Field evidence such as pillow structure indicates their eruption in a marine environment. Petrographic data reveal that the igneous mineralogy has been altered during post-magmatic hydrothermal alteration processes corresponding to greenschist- to lower amphibolite facies conditions with rarely preserved primary olivine and orthopyroxene. A 16-point Sm–Nd whole-rock isochron gives an age of 3352 ± 110 Ma for the timing of eruption of komatiite lavas. About 60% of the studied komatiite samples show Al-depletion whilst the remaining are Al-undepleted. The Al-depleted komatiites are characterised by high CaO/Al_2O_3 ratios (1.01–1.34) and low Al_2O_3/TiO_2 (5–16) whereas Al-undepleted komatiites show lower CaO/Al_2O_3 ratios (0.59–0.99) and higher Al_2O_3/TiO_2 (17–26). Trace element distribution patterns of komatiites suggest that most of the primary geochemical and Nd isotopic compositions are preserved with only minor influence of post-magmatic alteration processes and negligible crustal contamination. The chemical characteristics of Al-depleted komatiites, such as high $(Gd/Yb)_N$ together with lower HREE, Y, Zr and Hf, imply their derivation from deeper upper mantle with garnet (majorite?) involvement, whereas lower $(Gd/Yb)_N$ slightly higher HREE, Y, Zr and Hf suggest derivation from shallower upper mantle without garnet involvement. The observed chemical characteristics (CaO/Al_2O_3, Al_2O_3/TiO_2, MgO, Ni, Cr, Nb, Zr, Y, Hf, REE) indicate derivation of the komatiite magmas from different depths in a plume setting, whereas sub-contemporaneous felsic volcanism and TTG accretion can be attributed to an arc setting. In order to explain the spatial association of komatiite volcanism with contemporaneous mafic-felsic volcanism and TTG accretion we propose a combined plume-arc setting. Nd isotope data of the studied komatiites indicate depleted mantle reservoirs which may have evolved by early (>4.53 Ga) global differentiation of the silicate Earth as suggested by Boyet and Carlson [Boyet, M., Carlson, R.W., 2005. ^{142}Nd evidence for early (>4.53 Ga) global differentiation of silicate Earth. Science 309, 577–581] or extraction of continental crust during the early Archaean.

Keywords: Middle Archaean komatiites; Dharwar craton; Nd isotopes; Whole-rock geochemistry; Mantle evolution; Crustal growth

1. Introduction

Komatiites are ultramafic volcanic rocks (MgO >18 wt.%) that occur mainly in Archaean greenstone belts (Arndt and Nisbet, 1982). They form significant constituents of preserved Archaean crust and are crucial to our understanding the chemical and thermal evolution of the Archaean mantle, geodynamic processes and crustal growth patterns. During the last three decades komatiites have been extensively studied world wide particularly from Archaean greenstone belts of southern Africa, Canada, Australia, Brazil and Finland (e.g. Arndt, 1994, 2003; Jahn et al., 1982; Wilson and Carlson, 1989; Gruau et al., 1987; Lesher and Arndt, 1995; Fan and Kerrich, 1997; Grove et al., 1997; Parman et al., 1997; Kerrich et al., 1999; Polat et al., 1999; Chavagnac, 2004). The geodynamic context of komatiite melt generation and eruption have been the subjects of a lively debate (Arndt, 2003; Grove et al., 1997; Parman et al., 1997; Polat et al., 1999).

The Dharwar craton of southern India (Fig. 1) comprises vast areas of 3.36–2.7 Ga tonalitic–trondhjemitic–granodioritic (TTG) gneisses (regionally known as Peninsular gneisses), volcanic-sedimentary greenstone sequences of two generation (>3.0 Ga Sargur Group and 2.9–2.6 Ga Dharwar Supergroup) and 2.6–2.5 Ga calc-alkaline to high potassic granitoids (Chadwick et al., 2000; Jayananda et al., 2000, 2006 for review).

* Corresponding author. Fax: +91 80 23219295.
E-mail address: mjayananda@rediffmail.com (M. Jayananda).

0301-9268/$ – see front matter © 2007 Elsevier B.V. All rights reserved.
doi:10.1016/j.precamres.2007.07.010

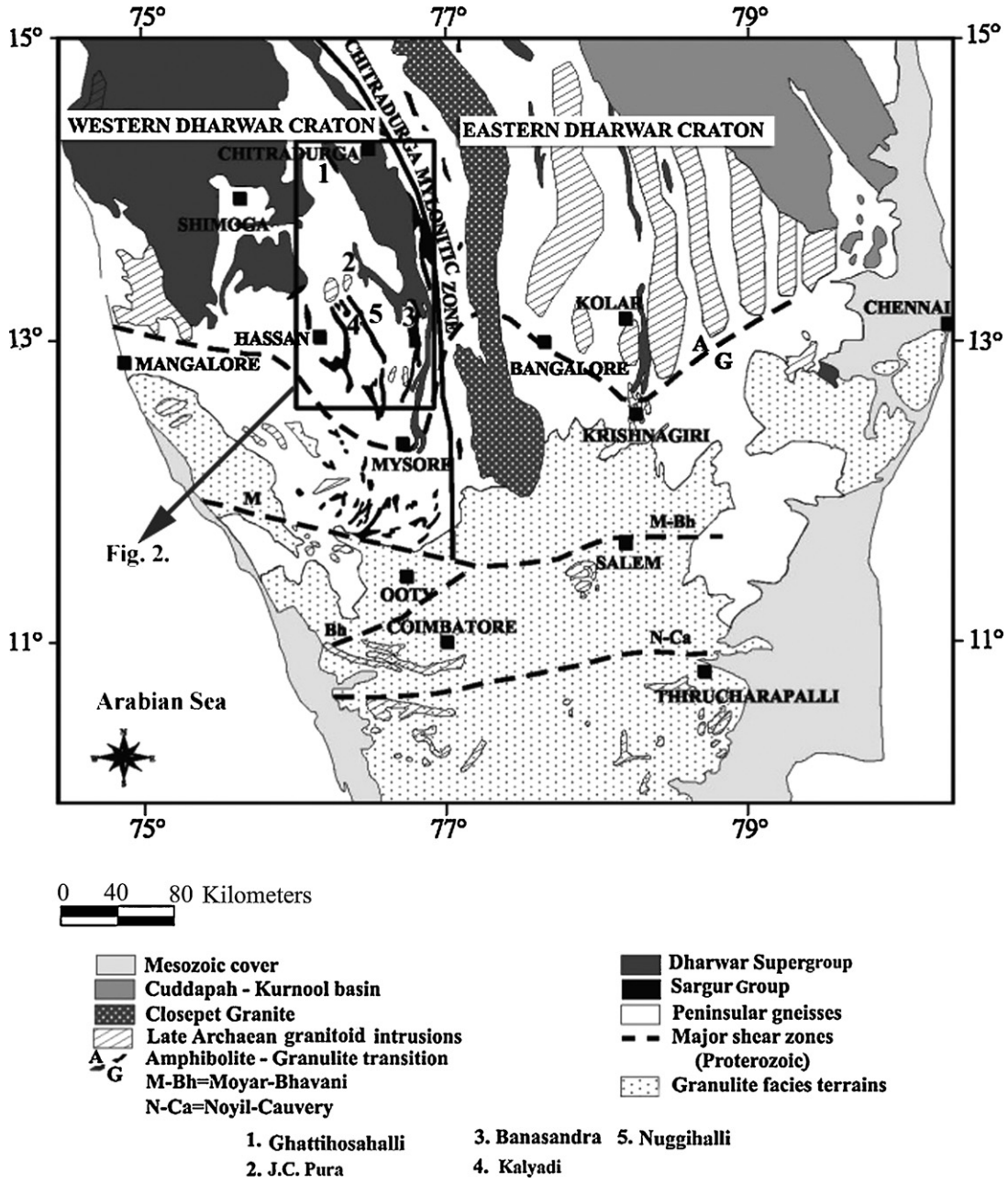

Fig. 1. Geological sketch map of the Dharwar craton showing the studied greenstone belts.

The craton is divided into two sub-blocks viz. Western Dharwar Craton (WDC) and Eastern Dharwar Craton (EDC) based on the nature and abundance of greenstones as well as the age of their surrounding basement and degree of regional metamorphism (Swaminath et al., 1976; Rollinson et al., 1981). The steep mylonitic zone along the eastern margin of the Chitradurga greenstone belt is considered as the boundary between the two crustal blocks. The WDC is dominated by older basement (>3.0 Ga TTG with interlayered Sargur Group rocks) which is unconformably overlain by 2.9–2.6 Ga Dharwar Supergroup volcano-sedimentary rocks/sequences (Meen et al., 1992; Nutman et al., 1992, 1996; Peucat et al., 1993, 1995; Ramakrishnan et al., 1994). The 2.61 Ga high potassic plutons form a minor component in the WDC (Jayananda et al., 2006). On the contrary the EDC comprises a younger (2.7 Ga) TTG basement with small remnants of >3.0 Ga TTG and thin elongated 2.7 Ga greenstone belts, and abundant 2.55–2.52 Ga calc-alkaline to high potassic intrusions (Balakrishnan et al., 1990, 1999; Krogstad et al., 1991; Jayananda et al., 2000; Chadwick et al., 2000; Chardon et al., 2002; Moyen et al., 2003).

The Sargur Group volcanic sequences in the WDC are dominated by ultramafic komatiite and tholeiitic rocks with subordinate felsic lava flows, whereas the Dharwar Supergroup volcanics contain abundant tholeiitic to felsic volcanics with subordinate basaltic komatiites. Previous geochronological studies were limited, mainly confined to Dharwar Super-

group of the WDC (Bhaskar Rao et al., 1992; Anil Kumar et al., 1996; Nutman et al., 1996) which was broadly correlated with late Archaean volcanics of the EDC (Balakrishnan et al., 1990; Zachariah et al., 1995; Naqvi et al., 2002; Manikyamba et al., 2005). These studies indicate extensive komatiite–tholeiite–boninite volcanism close to 2.7 Ga either in plume or arc environments. On the contrary, no detailed geochemical and isotope studies have been initiated on the Sargur Group greenstone volcanic sequences of the WDC, except for a Nd isotope study of anorthosites by Bhaskar Rao et al. (2000) and SHRIMP U–Pb zircon dating of felsic volcanic flows by Peucat et al. (1995) from the Holenarsipur schist belt. Studies on the Sargur Group volcanic sequences in the WDC mainly document field, petrographic and major element characteristics (Naqvi, 1981; Charan et al., 1988; Srikantia and Bose, 1985; Srikantia and Venkataramana, 1989; Srikantia and Rao, 1990; Venkata Dasu et al., 1991; Devapriyan et al., 1994; Subba Rao and Naqvi, 1999; Paranthaman, 2005). Their timing of eruption, their magmatic history including post-magmatic alteration processes and composition of mantle sources are not known. Furthermore, tectonic context of melt generation, whether related to plume or arc or plume-arc settings, is not known. Consequently, the main purpose of the paper is to present field, petrographic, Nd isotopic and whole-rock geochemical data for the komatiites of the Sargur-Group Ghattihosahalli, Jayachamarajapura (J.C. Pura), Banasandra, Kalyadi and Nuggihalli greentone belts in order to discuss timing of komatiite volcanism in the Sargur Group greenstone belts with respect to the accretion of the surrounding TTG basement, effects of post-magmatic alteration processes and crustal contamination, nature and composition of mantle sources and tectonic context of melt generation and eruption, Archaean mantle evolution and continental growth connection.

2. Geological setting

In the Dharwar craton the Sargur Group greenstone belts display well-preserved volcanic-sedimentary sequences. They usually comprise ultramafic–mafic volcanics of komatiite–tholeiite lineage, which towards higher levels give way to felsic volcanics, often of calc-alkaline lineage.

2.1. Ghattihosahalli belt

The Ghattihosahalli belt (Fig. 2) occurs along the western boundary of the Chitradurga belt. This belt is surrounded by 3.1 Ga TTG Peninsular gneisses in the west (Taylor et al., 1984) with poorly defined contact and overlain by the ~2.6 Ga old Chitradurga belt (Nutman et al., 1996). The volcanic-sedimentary sequence comprises ultramafic komatiites, amphibolites with interlayered fuchsite quartzite and barite beds (Radhakrishna and Sreenivasaiah, 1974). Viswanatha et al. (1977) first reported spinifex textured komatiites from this belt. Komatiites are generally interlayered with amphibolites. About 2 km south of Kummanghatta village boulders of spinifex textured komatiites are well exposed on the hilltop whereas massive exposures are confined to the lower levels.

2.2. J.C. Pura belt

The J.C. Pura belt (Fig. 2) is surrounded by 3.3 Ga old TTG to the south, overlain by the Kibbanahalli arm of the Chitradurga belt in the north and intruded by the 2.61 Ga Arsikere granite pluton (Chardon, 1997; Jayananda et al., 2006). The belt comprises komatiitic to tholeiitic volcanic sequences, cherty quartzites and banded iron formations. Detrital zircons from cherty quartzite yielded a single grain evaporation age of 3.2 Ga (Ramakrishnan et al., 1994). Massive to schistose komatiites are the most dominating rock type which show varying degrees of serpentinisation and carbonatization. They show spectacular pillow structures (Fig. 3), nodular or ocelli structures and quench textures (Venkata Dasu et al., 1991). Nodular or ocelli structures consist of spherical nodules or ocelli 1–2 cm in diame-

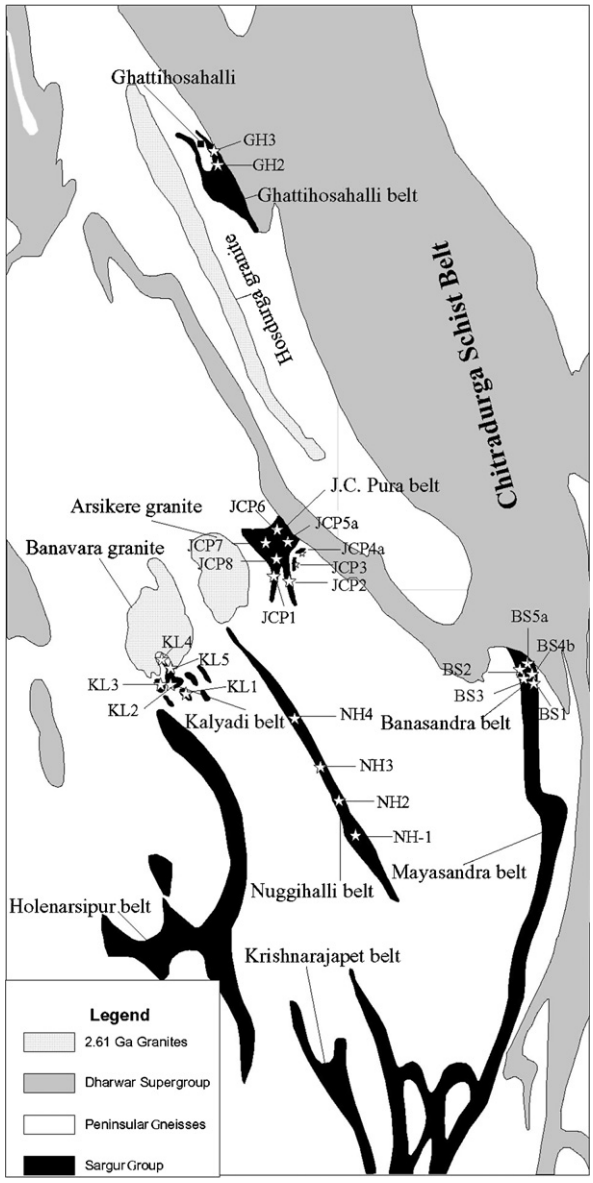

Fig. 2. Simplified geological sketch map of the studied Sargur Group greenstone belts in the western Dharwar craton including Ghattihosahalli, J.C. Pura, Banasandra, Kalyadi and Nuggihalli belts showing sample locations.

Fig. 3. Pillow structure from J.C. Pura belt (2 km NNE of Ramapura).

ter in fine-grained serpentine matrix. Elsewhere such structures have been interpreted as the products of liquid immiscibility, alteration or chilling processes during extrusion of lava (Arndt and Nisbet, 1982). The pillowed komatiites display polyhedral jointing where margins of pillows and polyhedrons developed chilled margins.

2.3. Banasandra area

Ultramafic volcanic lava flows of the Bansandra area are exposed in the southeastern margin of the Kibbanahalli arm of the Chitradurga greenstone belt (see Fig. 2) and have been described by Seshadri et al. (1981) and Srikantia and Bose (1985). They comprise massive serpentinites, pillowed to spinifex textured komatiites and hornblendites. The spinifex texture comprises criss-crossing sheafs of closely spaced and parallel blades of olivine (altered to serpentine) ranging from 3 to 8 cm long (Fig. 4). Pillowed komatiites are confined to the southern part of the area that underlies the spinifex textured komatiites. The pillows show chilled margins with occasional magnetite layers along boundary.

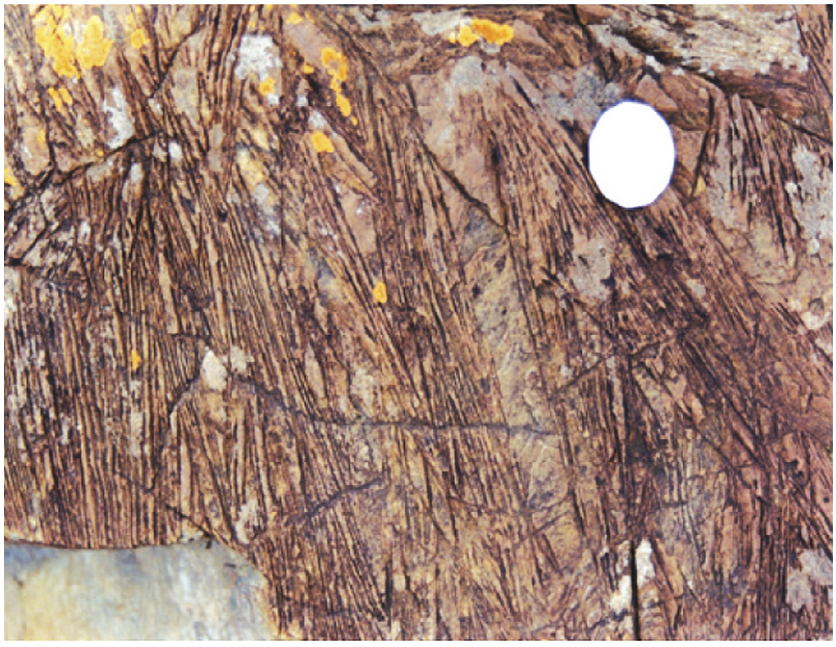

Fig. 4. Spinifex structure from Banasandra belt (1 km SSE of Kodihalli).

2.4. Kalyadi area

The volcanic-sedimentary greenstone sequences in the Kalyadi area (see Fig. 2) occur as small discontinuous bands interlayered with the Peninsular gneisses and intruded by the younger Banavara granite. They comprise metaultramafic–mafic volcanic rocks with minor sedimentary intercalations such as cherty quartzite and pelite (Subba Rao and Naqvi, 1999). The metavolcanic rocks consist of serpentinite, talc–tremolite–actinolite–chlorite schist and amphibolite. They display nodular structures (Arndt and Nisbet, 1982) which comprise spherical nodules 1–2 cm in diameter embedded in a fine-grained matrix.

2.5. Nuggihalli belt

The NNW-SSE trending Nuggihalli greenstone belt (see Fig. 2) comprises metaultramafic volcanics of peridotite to serpentinites, actinolite–tremolite–talc schists with minor amphibolites and metasediments. Recently Jaffri et al. (1997) have described spinifex textured komatiite in the northern part of the belt. The greenstone sequence contains intrusive ultramafic to mafic layered complexes with chromite layers spatially associated with the ultramafic rocks.

3. Petrography

The studied komatiites show diverse petrographic characteristics in texture, primary mineralogy and alteration features. They have been affected by greenschist facies to lower amphibolite facies metamorphism (Raase et al., 1986). Textures range from spinifex to cumulate typical of ultramafic lava flows. Spinifex blades are ranging from few mm to 8 cm in length. They are affected by hydrothermal alteration with rarely preserved primary igneous mineralogy. The hydrous alteration may be related to ocean-floor metamorphism or more likely to the regional tectono-metamorphic overprint (Raase et al., 1986). Carbonate is observed in several samples and occasionally forms network of tiny microscopic veins.

The petrographic characteristics of the studied komatiites are as follows.

The Ghattihosahalli samples comprise mainly serpentine and occasionally talc–tremolite with minor carbonate and opaques. Primary igneous minerals and textures are absent. The greenish to greenish grey coloured, massive to schistose J.C. Pura komatiite samples are dominated by serpentine–talc, serpentine–tremolite–talc, talc–chlorite assemblages. In rare instances relict olivine grains can be observed. Fine-grained serpentine forms the most abundant mineral. The Banasandra komatiites show spectacular spinifex texture where primary olivine blades are serpentinised. The common mineral assemblages include serpentine–talc, serpentine–talc–tremolite, serpentine–tremolite–actinolite–chlorite. The medium to fine-grained greyish green coloured Kalyadi komatiites shows the assemblages serpentine–talc–tremolite and actinolite–tremolite with minor hornblende. Minor carbonate and chlorite are common. The greenish to greyish green coloured komatiites of the Nuggihalli belt show olivine–enstatite–serpentine–chromite, actinolite–tremolite–serpentine–talc, clinopyroxene–hornblende, serpentine–chromite. Few samples contain primary minerals (olivine and enstatite) and show igneous textures. Fine-grained aggregates of carbonate are occasionally forming a network of tiny veins.

4. Geochronology

Geochronological data on the Sargur Group greenstone belts is rather scanty. U–Pb SHRIMP ages of detrital zircons from metapelitic rocks of the Holenarsipur belt indicate 3090–3580 Ma for the provenance (Nutman et al., 1992). Further northeast in the Banavara area detrital zircons from quartzites yielded SHRIMP U–Pb ages between 2940 and 3230 Ma (Nutman et al., 1992) whilst detrital zircons from cherty quartzites of adjoining J.C. Pura belt also indicate a provenance age of ca. 3230 Ma (Ramakrishnan et al., 1994). Furthermore, a magmatic stage, synchronous with the sedimentary deposits, is determined by U–Pb SHRIMP zircon data from a felsic volcanic flow of the Holenarsipur belt at 3298 ± 7 Ma (Peucat et al., 1995). The timing of mafic–ultramafic volcanism in the Sargur Group is not directly constrained. In fact, Drury et al. (1987) obtained a Sm–Nd whole isochron age of 2620 ± 55 Ma for mafic volcanics from the upper part of the Holenarsipur belt which would belong to the Dharwar Supergroup. However, the Sm–Nd system could have been reset by the late Archaean greenschist facies overprint of the mafic volcanics, thus implying an older protolith age (see discussion in Peucat et al., 1995).

In order to define the timing of ultramafic volcanism in the Sargur Group in the WDC, we have analysed 20 komatiite samples from the Ghattihosahalli, J.C. Pura, Banasandra, Kalyadi and Nuggihalli greenstone belts for Sm–Nd isotopes (Table 1). Analytical methods for Sm–Nd isotope analysis are presented in Appendix A.

All the analyzed komatiite samples are ultramafic in composition and display a large variation in $^{147}Sm/^{144}Nd$ values. This is also manifested by the distinct LREE patterns shown in Fig. 10a–e. Sixteen of the twenty analysed whole-rock samples define an isochron age of 3352 ± 110 Ma ($\pm 2\sigma$) with an initial $^{143}Nd/^{144}Nd$ ratio of 0.50838 ± 0.0015 ($\pm 2\sigma$) and a corresponding $\varepsilon_{Nd}(t)$ value of $+2.0 \pm 3.0$ for a MSWD of 3.1 (Fig. 5). There is no correlation between the $^{143}Nd/^{144}Nd$ ratios measured and 1/Nd of samples belonging to the isochron, and thus no evidence for a mixing line. The isochron is mainly defined by the J.C. Pura samples which display a large $^{147}Sm/^{144}Nd$ spread (0.1447–0.2194), the six samples yield an age of 3384 ± 200 Ma (MSWD = 1.8; figure is not given). Five samples of the Kalyadi and adjoining Nuggihalli belts representing evolved magmas also define an isochron age of 3284 ± 310 Ma (MSWD = 3.7; figure is not given). The four discarded samples show disturbed REE patterns which probably were caused by fluid-induced alteration processes during metamorphism. The three obtained isochron ages are within the range of analytical error. As komatiites from different belts of the Sargur Group are included in the calculation, the isochron

Table 1
Sm–Nd isotopic data for respresentative komatiites from Sargur Group greenstone belts of the Western Dharwar Craton

Samples	Sm (ppm)	Nd (ppm)	$^{147}Sm/^{144}Nd$	$^{143}Nd/^{144}Nd$	Error ($\pm 2\sigma m$)	$\varepsilon(0)$ ($t = 0$ Ma)	TDM1 (in Ma) ($\varepsilon_0DM = +8$)	TDM2 (in Ma) ($\varepsilon_0DM = +9.5$)	$\varepsilon_{Nd}(t)$ ($t = 3352$ Ma)
Ghattihosahalli									
GH-2	0.613	2.483	0.1493	0.511859	0.000004	−15.2	2802	2977	5.0
GH-3	0.602	2.158	0.1686	0.512159	0.000005	−9.39	2992	3241	2.6
J.C. Pura									
JCP-1	0.196	0.642	0.1851	0.512496	0.000004	−2.81	2935	3328	2.1
JCP-4a	2.570	10.74	0.1447	0.511569	0.000005	−20.9	3248	3410	1.3
JCP-5a	0.507	1.655	0.1851	0.512498	0.000004	−2.77	2924	3317	2.2
JCP-6	0.283	0.801	0.2136	0.513148	0.000005	9.91	–	–	2.7
JCP-7	0.184	0.617	0.1801	0.512351	0.000004	−5.64	3149	3483	1.5
JCP-8a	0.290	0.800	0.2194	0.513203	0.000005	11.0	–	–	1.3
Banasandra									
BS-1	0.200	0.562	0.2150	0.513179	0.000004	10.5	–	–	2.7
BS-2	0.295	0.812	0.2199	0.513298	0.000004	12.8	–	–	2.9
BS-3	0.193	0.524	0.2231	0.513296	0.000005	12.8	–	–	1.5
BS-4b	0.358	0.891	0.2431	0.514037	0.000004	27.2	–	–	7.4
BS-5a	0.519	1.320	0.2377	0.513682	0.000004	20.3	–	–	2.8
Kalyadi									
KL-2	2.378	9.863	0.1458	0.511587	0.000004	−20.5	3260	3425	1.2
KL-3	0.444	1.299	0.2068	0.512986	0.000006	6.75	–	–	2.4
KL-4	0.434	1.147	0.2290	0.513383	0.000004	14.5	–	–	0.7
KL-5	0.137	0.345	0.2401	0.513466	0.000009	16.1	–	–	−2.5
Nuggihalli									
NH-1	2.050	6.447	0.1922	0.512616	0.000004	−0.47	3057	3579	1.5
NH-2	0.165	0.677	0.1475	0.511873	0.000005	−15.0	2695	2865	6.1
NH-3	0.206	0.571	0.2177	0.513126	0.000004	9.48	–	–	0.5

correlation suggests that all the volcanic sequences were derived at the same time from the same source. Alternatively it could indicate that different komatiites were deposited within a short time interval with close initial Nd isotopic compositions. Consequently the 16 point Sm–Nd whole-rock isochron age of 3352 ± 110 Ma is interpreted as the age of the komatiite volcanism or alternatively as an average for timing of komatiitic volcanism in the Sargur Group greenstone belts of the WDC.

The obtained age for komatiites is sub-contemporaneous with respect to the accretion of the oldest dated TTG basement and also felsic volcanic flows of the Sargur Group in the WDC.

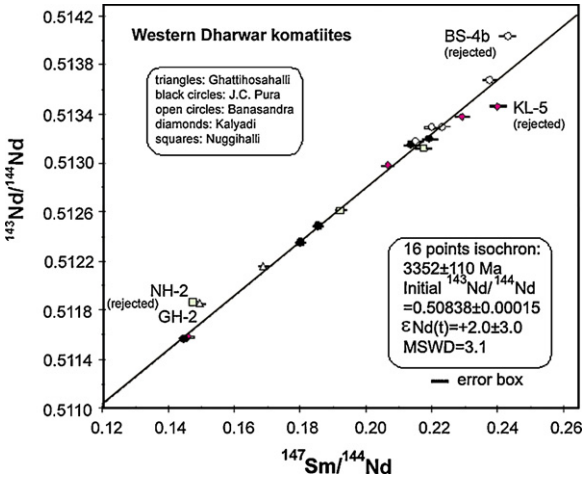

Fig. 5. Sm–Nd whole-rock isochron of komatiites from the Sargur Group greenstones in the WDC.

5. Geochemistry

5.1. Major and trace elements

Major and trace element compositions together with element ratios of the komatiites from WDC are given in Table 2 and the analytical procedures presented in Appendix A. The major element oxides used in different plots are on anhydrous basis recalculated to 100. The samples show significant variation in major and trace element contents. The distinctions between komatiites and komatiitic basalts are based on MgO contents (Arndt and Nisbet, 1982). Most of the samples are komatiites with MgO 22.9–42.3 wt.%. Two samples are komatiitic basalts (MgO = 11.9–17.2). This is reflected in the Al_2O_3–$Fe_2O_3 + TiO_2$–MgO (Fig. 6) triangular diagram (Jensen, 1976, as modified by Viljoen et al., 1982) and the CaO–MgO–Al_2O_3 (Fig. 7) diagram (Viljoen et al., 1982). The WDC komatiites show compositional characteristics of both, the Al-depleted Barberton-type ($CaO/Al_2O_3 = 1.01$–1.34; $Al_2O_3/TiO_2 = 5$–16) and the Al-undepleted Munro type ($CaO/Al_2O_3 = 0.59$–0.99; $Al_2O_3/TiO_2 = 17$–26).

On the Harker's binary diagrams of major element oxides versus MgO, Al_2O_3, TiO_2, CaO, P_2O_5, SiO_2 and Fe_2O_3 exhibit moderate to strong negative correlations whereas alkalies show scattering (Fig. 8). Among trace elements, Ni displays a positive correlation, whereas Y and Zr show moderate negative correlations with MgO (Fig. 9). Cr forms clusters for distinct groups suggesting chromite and olivine fractionation whereas Rb and Ba show a large spread (see Fig. 9).

Table 2
Major and trace element data for respresentative komatiites from Sargur Group greenstone belts of western Dharwar craton

Oxide	GH-2	GH-3	JCP-1	JCP-2	JCP-3	JCP-4a	JCP-5a	JCP-6	JCP-7	JCP-8	BS-1	BS-2
SiO_2	42.40	42.00	43.50	43.15	53.90	44.04	42.33	42.24	42.04	42.85	41.34	41.81
TiO_2	0.24	0.26	0.19	0.27	0.46	0.27	0.23	0.29	0.17	0.25	0.20	0.24
Al_2O_3	1.20	1.30	3.35	4.53	8.91	5.95	2.03	4.34	2.36	3.40	2.92	2.15
Fe_2O_3	8.07	9.01	9.25	9.77	7.91	10.36	10.21	10.96	10.29	10.16	8.15	8.03
MnO	0.14	0.16	0.12	0.16	0.14	0.25	0.23	0.17	0.09	0.16	0.10	0.14
MgO	41.33	39.27	37.05	34.14	11.94	29.90	37.85	34.58	40.02	36.39	41.94	41.19
CaO	1.58	1.74	2.78	4.40	8.78	5.34	2.06	4.12	1.39	2.42	2.03	2.01
Na_2O	0.02	0.01	0.02	0.17	2.75	0.44	0.02	0.03	0.02	0.02	0.02	0.02
K_2O	0.01	0.01	0.01	0.03	0.14	0.07	0.01	0.01	0.01	0.01	0.01	0.01
P_2O_5	0.08	0.02	0.02	0.02	0.05	0.02	0.02	0.02	0.01	0.02	0.02	0.02
LOI	5.73	6.36	5.12	4.15	5.79	4.73	5.05	4.12	5.14	5.14	4.62	5.16
Total	100.80	100.14	101.41	100.79	100.77	101.37	100.04	100.89	101.54	100.82	101.35	100.78
Ba	15	5	16	6	7	4	6	N.D.	15	9	4.9	3.4
Cr	1208	1338	2011	2659	427	1594	4395	2316	1663	3999	1847	1803
Nb	0.32	0.75	1.72	N.D.	3.00	3.00	0.72	N.D.	0.50	1.11	2.57	0.14
Ni	3145	3177	2172	1377	188	1143	2174	1542	2500	1596	2332	2361
Rb	9.00	6.00	2.90	1.00	N.D.	1.10	1.21	N.D.	1.92	0.90	1.20	1.10
Sr	16.3	14.6	22	55	89	14	18	125	23	11	10	11
V	78	84	84	132	190	183	128	135	108	132	110	105
Y	3	3	4	4	10	5	6	6	2	6	3	8
Zn	44	63	60	54	26	116	104	65	41	77	52	71
Zr	16	13	10	17	17	15	19	14	4	7	8.1	5.4
Th	0.03	0.10	0.10				0.14		0.03	0.07	0.05	0.02
U	0.01	0.05	0.09				0.02		0.02	0.18	0.02	0.01
Hf	0.04	0.09	0.09				0.05		0.06	0.06	0.18	0.04
Pb	1.78	1.89	2.16				1.21		0.82	0.96	0.69	1.24
Ti	1920	2080	1520				1840		1360	2000	1600	1920
La	1.17	1.21	0.44				0.94		0.56	0.41	0.26	0.46
Ce	3.05	2.90	1.90				3.25		1.98	1.81	1.22	1.08
Pr	0.43	0.38	0.12				0.28		0.12	0.15	0.09	0.13
Nd	2.60	2.22	0.72				1.63		0.63	0.91	0.62	0.88
Sm	0.59	0.76	0.27				0.58		0.22	0.32	0.25	0.36
Eu	0.28	0.18	0.06				0.15		0.07	0.06	0.12	0.14
Gd	0.59	0.66	0.26				0.56		0.26	0.39	0.26	0.43
Tb	0.08	0.13	0.06				0.12		0.06	0.09	0.07	0.10
Dy	0.42	0.59	0.35				0.61		0.27	0.41	0.40	0.54
Ho	0.07	0.13	0.10				0.15		0.06	0.10	0.09	0.12
Er	0.25	0.32	0.28				0.40		0.16	0.25	0.21	0.32
Tm	0.03	0.03	0.05				0.05		0.03	0.04	0.04	0.05
Yb	0.21	0.21	0.23				0.36		0.21	0.29	0.21	0.30
Lu	0.04	0.04	0.06				0.05		0.03	0.04	0.04	0.05
ΣREE	9.81	9.77	4.90				9.12		4.68	5.27	3.87	4.94
$Fe_2O_3/Fe_2O_3 + MgO$	0.16	0.19	0.20	0.22	0.40	0.26	0.21	0.24	0.20	0.22	0.16	0.16
CaO/Al_2O_3	1.32	1.34	0.83	0.97	0.99	0.90	1.01	0.95	0.59	0.71	0.70	0.93
Al_2O_3/TiO_2	5.00	5.00	17.63	16.78	19.37	22.04	8.83	14.97	13.88	13.60	14.60	8.96
$(Gd/Yb)_N$	2.21	2.48	0.91				1.26		1.01	1.09	1.01	1.14
Nb/Th	11.32	7.22	17.88				5.26		19.96	15.46	47.67	8.81
Nb/U	22.64	14.73	18.45				29.83		26.26	6.08	171.60	15.67
Nb/La	0.27	0.62	3.93				0.76		0.89	2.73	10.09	0.31
$(La/Sm)_N$	1.21	0.97	0.99				0.98		1.54	0.78	0.61	0.79
$(La/Yb)_N$	3.60	3.75	1.25				1.73		1.75	0.93	0.81	1.01
Ti/Zr	120	160	152				97		340	270	197	355

Oxide	BS-3	BS-4b	BS-5a	KL-1	KL-2	KL-3	KL-4	KL-5	NH-1	NH-2	NH-3	NH-4
SiO_2	41.55	42.28	46.56	50.28	50.60	46.86	38.91	46.41	41.94	41.34	42.51	38.20
TiO_2	0.23	0.19	0.25	0.40	0.27	0.38	0.40	0.27	0.46	0.24	0.36	0.22
Al_2O_3	2.63	3.14	4.62	7.90	6.34	5.19	4.95	5.12	4.84	5.04	3.52	4.91
Fe_2O_3	7.13	7.20	8.51	11.40	9.74	7.01	12.38	5.13	10.04	10.69	10.08	10.95
MnO	0.10	0.13	0.13	0.19	0.19	0.18	0.17	0.08	0.18	0.08	0.15	0.05
MgO	42.41	38.35	30.35	17.24	22.91	30.87	32.97	32.31	32.98	34.95	33.62	37.30
CaO	1.68	3.38	4.44	6.83	5.86	4.34	6.27	6.78	3.11	3.07	4.20	4.01
Na_2O	0.01	0.09	0.21	0.47	0.46	0.42	0.01	0.11	0.13	0.07	0.35	0.01

Table 2 (*Continued*)

Oxide	GH-2	GH-3	JCP-1	JCP-2	JCP-3	JCP-4a	JCP-5a	JCP-6	JCP-7	JCP-8	BS-1	BS-2
K_2O	0.01	0.01	0.02	0.27	0.06	0.04	0.01	0.05	0.02	0.01	0.08	0.01
P_2O_5	0.02	0.01	0.02	0.03	0.04	0.02	0.02	0.01	0.02	0.01	0.02	0.01
LOI	4.90	5.88	5.67	5.07	3.94	4.73	4.59	4.72	6.72	5.02	5.80	4.98
Total	100.67	100.66	100.78	100.08	100.41	100.04	100.68	100.99	100.44	100.52	100.69	100.65
Ba	5	10	11	N.D.	10	10	6	13	9	8	12	22
Cr	1614	2193	2138	1009	1969	2209	3597	2923	2702	>4400	2709	3374
Nb	1.49	2.00	0.22	N.D.	1.20	0.56	1.10	1.93	1.89	2.44	0.67	N.D.
Ni	2619	1559	1313	289	866	1388	1305	1396	1960	1652	1544	1564
Rb	0.90	3	3	1	1.60	1.70	1	1.20	0.90	2	0.60	0.59
Sr	18	9	24	106	23	48	45	23	35	12	20	N.D.
V	84	117	141	294	188	146	261	108	160	217	130	123
Y	4	5	5	10	7	3	5	4	6	5	4	5
Zn	37	70	48	80	61	59	58	60	69	109	51	22
Zr	5	10	14	23	20	21	25	13	27	10	9	9
Th	0.02		0.04		0.85	0.07	0.16	0.09	1.03	0.16	0.08	
U	0.01		0.01		0.13	0.01	0.15	0.01	0.11	0.00	0.06	
Hf	0.15		0.18		0.87	0.19	0.12	0.25	1.19	0.07	0.23	
Pb	0.99		2.04		2.33	30.59	2.76	1.76	3.61	1.62	0.83	
Ti	1840		3600		4560	3920	4400	4560	3680	2720	2880	
La	0.33		0.41		8.56	0.82	0.54	0.21	3.14	0.90	0.43	
Ce	0.77		1.18		16.37	1.77	1.31	0.24	7.86	1.36	0.87	
Pr	0.09		0.20		2.09	0.26	0.19	0.07	1.10	0.12	0.10	
Nd	0.63		1.50		10.51	1.40	1.16	0.33	6.53	0.56	0.61	
Sm	0.24		0.61		2.79	0.53	0.43	0.15	2.20	0.19	0.23	
Eu	0.10		0.18		0.68	0.17	0.11	0.05	0.70	0.03	0.09	
Gd	0.27		0.77		2.61	0.61	0.46	0.21	2.24	0.17	0.31	
Tb	0.08		0.17		0.51	0.14	0.11	0.06	0.49	0.04	0.08	
Dy	0.38		1.07		2.85	0.83	0.52	0.44	2.49	0.26	0.49	
Ho	0.10		0.22		0.65	0.18	0.12	0.13	0.58	0.08	0.15	
Er	0.26		0.66		1.86	0.53	0.29	0.41	1.62	0.24	0.42	
Tm	0.03		0.10		0.26	0.08	0.04	0.06	0.25	0.04	0.04	
Yb	0.22		0.60		1.75	0.53	0.25	0.27	1.45	0.32	0.33	
Lu	0.04		0.09		0.30	0.08	0.04	0.06	0.24	0.05	0.08	
ΣREE	3.55		7.76		51.77	7.92	5.59	2.71	30.88	4.40	4.24	
$Fe_2O_3/Fe_2O_3 + MgO$	0.14	0.16	0.22	0.40	0.30	0.19	0.27	0.14	0.23	0.23	0.23	0.23
CaO/Al_2O_3	0.64	1.08	0.96	0.86	0.92	0.84	1.27	1.32	0.64	0.61	1.19	0.82
Al_2O_3/TiO_2	11.43	16.53	18.48	19.75	23.48	13.66	12.38	18.96	10.52	21.00	9.78	22.32
$(Gd/Yb)_N$	1.01		1.03		1.20	0.92	1.47	0.64	1.24	0.43	0.76	
Nb/Th	64.87		6.29		1.40	7.85	6.77	21.65	1.83	15.61	8.79	
Nb/U	186.50		27.50		9.57	39.79	7.35	148.23	17.34	1217.50	11.93	
Nb/La	4.47		0.54		0.14	0.68	2.06	9.00	0.60	2.70	1.55	
$(La/Sm)_N$	0.83		0.41		1.87	0.95	0.75	0.87	0.87	2.85	1.13	
$(La/Yb)_N$	1.02		0.45		3.24	1.02	1.40	0.52	1.44	1.84	0.87	
Ti/Zr	368		257		228	186	176	350	136	272	320	

Ordinary chondrite values used for normalising our data are Leedy chondrite data divided by 1.2 with values for Pr, Tb, Ho and Tm interpolated after Taylor and Gordon (1977). The studied komatiites are characterized by variable total REE contents (2.70–51.7 ppm, Table 2). The Ghattihosahalli samples display slightly fractionated REE patterns with $(Gd/Yb)_N = 2.48–2.21$ (Fig. 10a). The J.C. Pura samples show low to moderate total REE (4.8–9.1 ppm) and display flat REE patterns with $(Gd/Yb)_N = 1.26–0.92$ (Fig. 10b) with either minor negative Eu anomalies or without Eu anomalies. All the four analysed samples show positive Ce anomalies. The Banasandra komatiites also show flat REE patterns with $(Gd/Yb)_N$ ratios of 1.01–1.14 and either slight positive or negative Eu anomalies (Fig. 10c).

The Kalyadi samples show large variation in total REE contents (2.71–51.77 ppm). Sample KL-5 displays sub-chondritic total REE (2.71 ppm). The REE pattern is characterised by slightly enriched HREE $(Gd/Yb)_N = 0.64$ and depletion in LREE $(La/Sm)_N = 0.86$ and MREE (Fig. 10d). Sample KL-4 also shows a chondritic flat REE pattern with a minor negative Eu anomaly and HREE fractionation $(Gd/Yb)_N = 1.47$. Sample KL-2 has the highest total REE (51.7 ppm) of all the studied samples and shows HREE fractionation with $(Gd/Yb)_N = 1.2$.

Among the Nuggihalli komatiites (Fig. 10e), sample NH-2 shows weak LREE fractionation $(La/Sm)_N = 2.8$, a weak negative Eu anomaly and enriched HREE with $(Gd/Yb)_N = 0.42$. The other samples show variable total REE (4.2–30.8 ppm) but relatively flat REE patterns with $(Gd/Yb)_N = 0.76–1.24$.

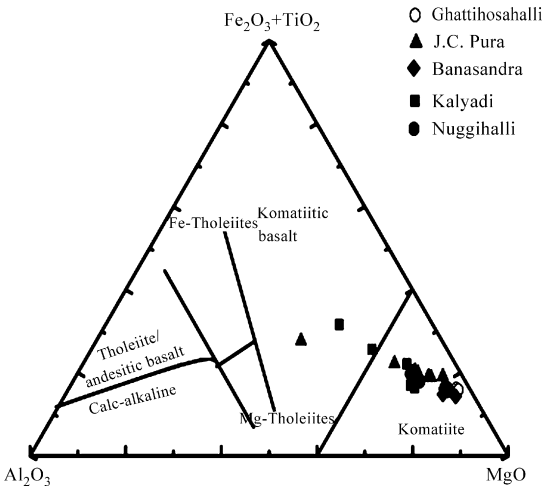

Fig. 6. Al_2O_3–Fe_2O_3 + TiO_2–MgO triangular plot (Jensen, 1976 modified by Viljoen et al., 1982).

The primitive mantle normalized multielement patterns of the komatiites are variable in LILE and Nb, but relatively uniform in Ti, Zr, Hf and REE (Fig. 11a–f). The Ghattihosahalli (Fig. 11a), J.C. Pura (Fig. 11b) and Banasandra (Fig. 11c) samples display relatively uniform, parallel flat patterns except in LILE and Nb. Few samples show small negative Nb anomalies whereas other samples show positive Nb anomalies. Rb and Ba show crossing relations being either depleted or slightly enriched whereas Pb is enriched.

The Kalyadi and Nuggihalli samples exhibit more complex patterns. Three broad groups can be recognized:

a. Samples (KL-3, KL-4 and NH-3) show relatively parallel patterns in REE including Hf and Zr but are slightly depleted compared to primitive mantle (Fig. 11d). LIL elements including U and Th show crossing. They also display weak negative Hf anomalies but flat REE pattern including Y.

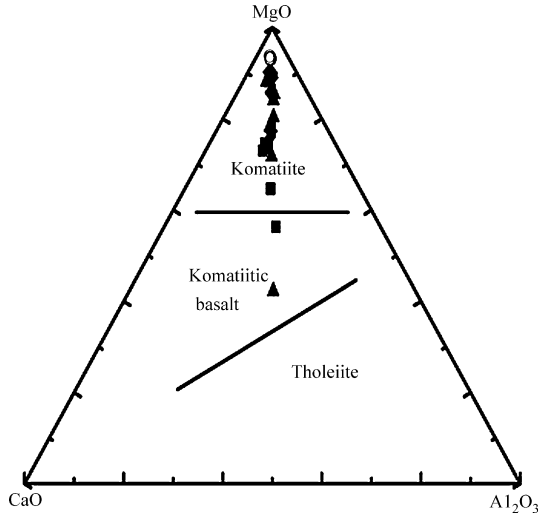

Fig. 7. CaO–MgO–Al_2O_3 triangular diagram (Viljoen et al., 1982).

b. Samples (KL-2 and NH-1) are characterized by nearly parallel patterns with high LILE, REE and show weakly negative Nb and Ti anomalies without any significant Hf and Zr anomalies (Fig. 11e).
c. Samples (KL-5 and NH-2) exhibit a strong depletion of U, LREE and MREE $(Gd/Yb)_N = 0.64–0.43$ with uniformly depleted HREE. They show positive Nb and negative Hf anomalies (Fig. 11f).

6. Discussion

6.1. Effects of alteration and metamorphism

The studied Sargur Group komatiites of the WDC are mainly affected by hydrothermal alteration and greenschist facies metamorphism with rarely preserved primary olivine and clinopyroxene. The mineral assemblages comprising dominant serpentine, actinolite–tremolite, talc, and chlorite indicate metamorphic recrystallisation under low-grade conditions. On the other hand, the occurrence of tiny carbonate vein networks implies further fluid induced hydrothermal alteration processes. In the petrogenetic discussion only least altered samples were considered and samples with very high loss of ignition (LOI) discarded. Considering the metamorphic mineralogy, the discussion here emphasises on geochemical data of relatively immobile elements such as REE and HFSE.

The majority of samples show uniform Al_2O_3/TiO_2, $(Gd/Yb)_N$ ratios with relatively smooth REE patterns. Primitive mantle-normalised multi-element diagrams indicate that the trace element systematics of the komatiites was not affected by the low-grade hydration processes. This finding is also supported by relatively smooth trends of SiO_2, TiO_2, Al_2O_3, P_2O_5 and CaO against MgO. On the other hand, scattering of alkalies, Ba and Rb indicate their mobilisation during the alteration processes.

All the J.C. Pura samples display positive Ce anomalies (see Fig. 10b), while only one sample of Banasandra displays a positive Ce anomaly. On the contrary, one Kalyadi sample shows depletion of LREE and strong negative Ce anomaly. Studies indicate that Ce anomalies occur in response to oxidation of Ce^{3+} to Ce^{4+} and precipitation of Ce^{4+} from solution as CeO_2 (e.g. Braun et al., 1993). Consequently the positive Ce anomalies observed in the J.C. Pura and Banasandra komatiites could be probably related to precipitation by circulating fluid phase in an oxidizing environment, which is supported by the presence of tiny carbonate vein networks. On the other hand, the Ce depletion observed in komatiites of the Kalyadi belt (which represents a slightly lower structural level in the crust) could be attributed to removal of Ce by circulating fluids during metamorphism. Few samples which are characterised by high MgO contents display either slight positive or negative Eu anomalies, implying that most magnesium rich rocks were also susceptible to alteration (cf. Lecuyer et al., 1994; Fan and Kerrich, 1997). Eu anomalies are also observed in komatiites of other cratons around the world and are generally attributed to secondary alteration processes (Sun and Nesbitt, 1978; Ludden et al., 1982; Arndt, 1994). Recent Nd and O isotope studies of komatiite flows from different cratons (Gruau et al., 1992; Lecuyer et al.,

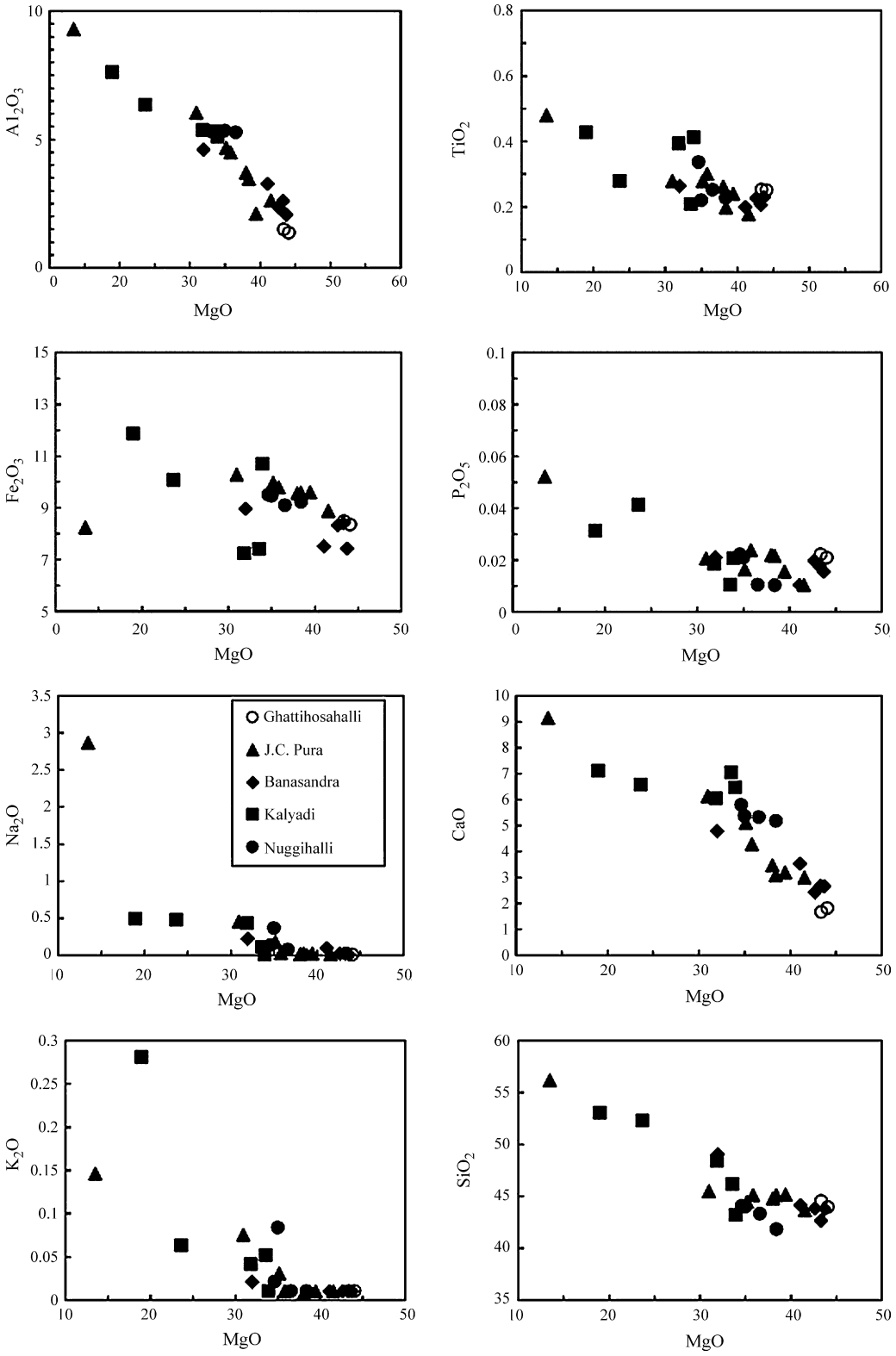

Fig. 8. Harker's binary diagrams showing selected major element oxides vs. MgO.

1994; Lahaye et al., 1995) indicate mobility of Nd and LREE during metamorphism and hydrothermal alteration processes.

The majority of whole-rock $^{143}Nd/^{144}Nd$ and $^{147}Sm/^{144}Nd$ values define a linear array suggesting preservation of Sm–Nd isotope systematics in most cases except four samples that form a scatter. Published *P–T–t* paths and isotopic age data indicate that the WDC was affected by earlier thermal events close to 3.0 and 2.6 Ga (Jayananda and Peucat, 1996; Jayananda et al., 2006). Fluid flux associated with these thermal events probably caused the mobility of Rb, Ba, Th and LREE. In conclusion

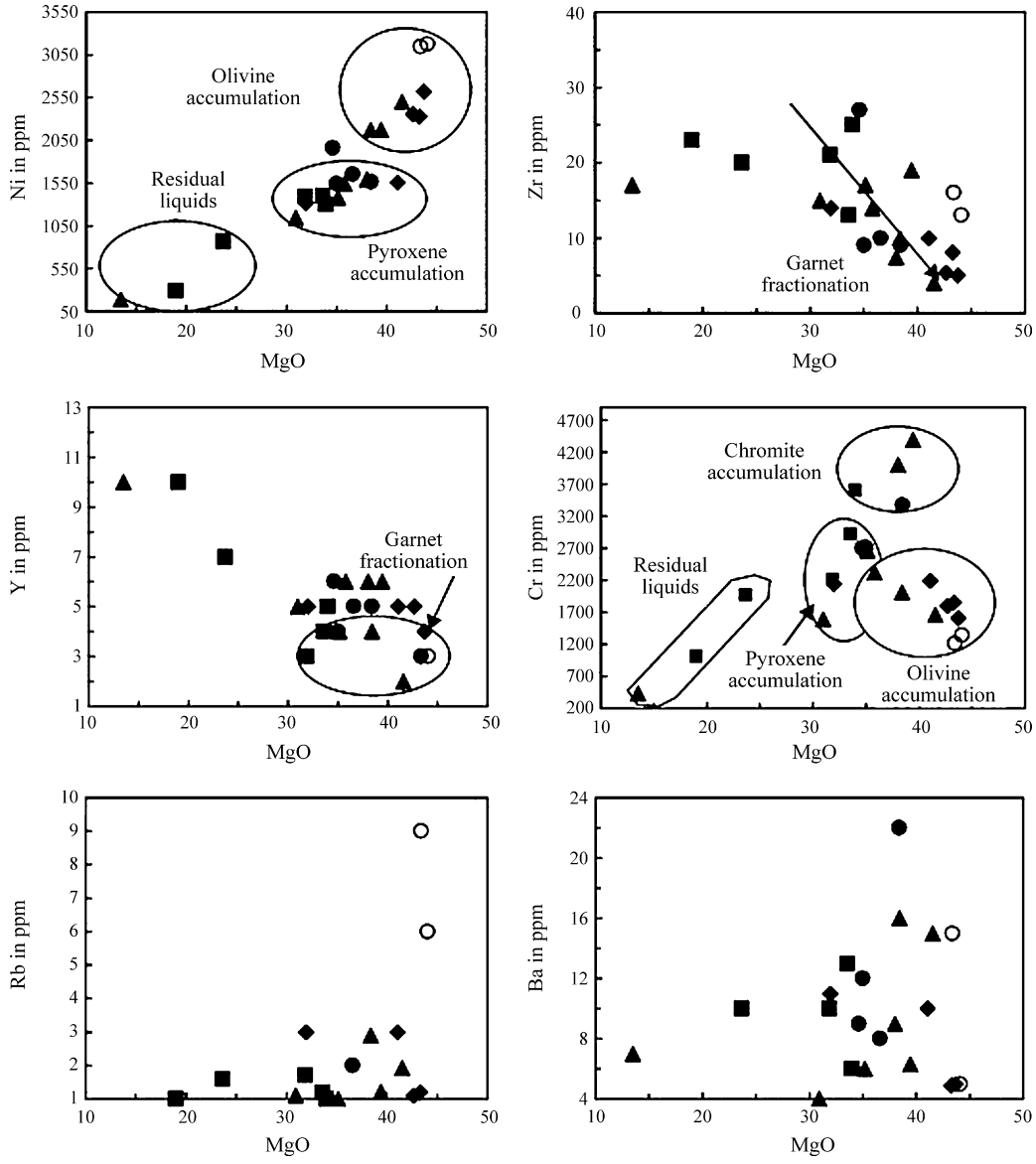

Fig. 9. Harker's binary diagram for selected trace elements against MgO (symbols are same as in Fig. 6).

most of the studied komatiites in the WDC were not affected by large-scale alteration processes and thus are suited to constrain the composition of the Archaean mantle.

6.2. Contamination

Relative to primitive mantle, continental crust is characterised by high LREE, low Nb, P, Ti and Ti/Zr ratios. The majority of the komatiite samples does not show LREE enrichment, negative Nb anomalies on primitive mantle-normalised multi-element diagrams, low Ti/Zr ratios and negative $\varepsilon_{Nd}(t)$ values. However, two samples display LREE, U, Th, Zr and Hf enrichment and pronounced negative Ti–Nb anomalies, but show positive ε_{Nd} values (1.2–1.5 at 3.352 Ga) which rules out crustal contamination. Given this fact we preclude contamination of continental crust and assume that the observed trace element compositions reflect their source regions. Although one sample (KL-5) exhibits a negative ε_{Nd} value (−2.5 at 3.35 Ga), the strong depletion of LREE and MREE and positive Nb anomaly rules out crustal contamination and possibly can be related to alteration.

6.3. Magmatic fractionation

The majority of the samples from different greenstone belts in the WDC are peridotitic komatiites and few samples are basaltic komatiite in composition. Irrespective of the significant variation in terms of metamorphic mineralogy, texture, major and trace element compositions, they define moderate to strong linear trends on binary diagrams indicating that their magmas evolved by differentiation processes. Peridotitic komatiites plot co-linearly with basaltic komatiites on binary diagrams of Al_2O_3, SiO_2, TiO_2, CaO, P_2O_5 versus MgO albeit to higher absolute concentrations suggestive of a co-magmatic origin by olivine and to some extent pyroxene fractionation (see Fig. 8).

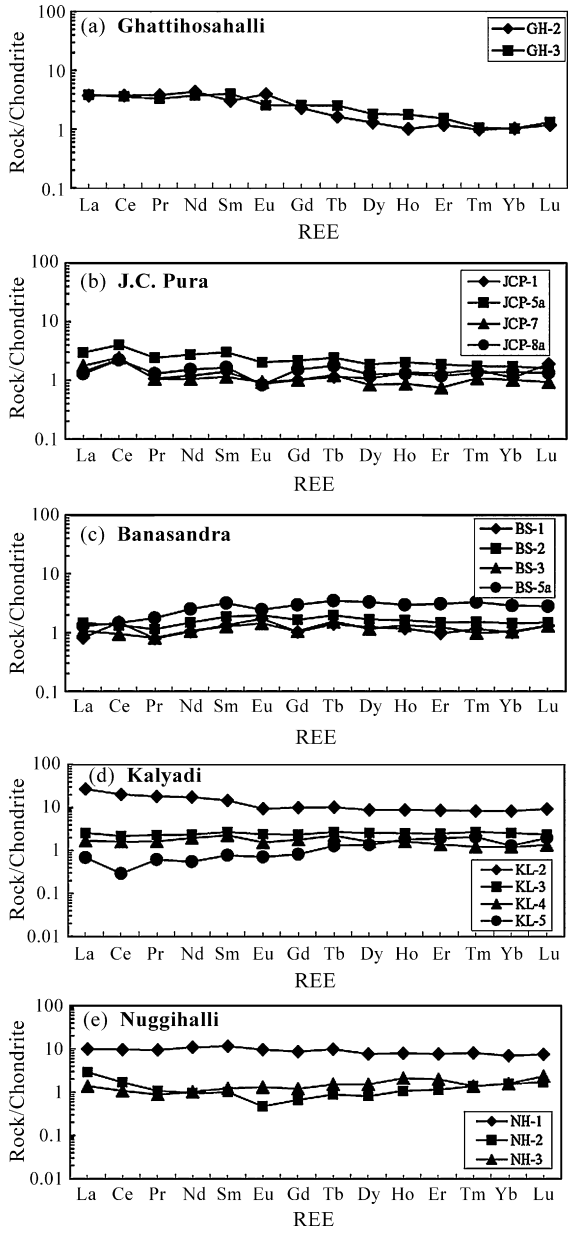

Fig. 10. (a–c) Chondrite normalized REE patterns of Ghattihosahalli, J.C. Pura and Banasandra komatiites. (d and e) Chondrite normalized REE patterns of Kalyadi and Nuggihalli komatiites.

The positive correlation of MgO with Ni (see Fig. 9) but negative correlation with Al_2O_3 and TiO_2 suggests that primary MgO contents were largely controlled by fractionation or accumulation of olivine. The negative correlation of Zr and Y with MgO implies garnet involvement. On the other hand, large spread of K_2O, Ba and Rb (see Figs. 8 and 9) indicates mobility of these elements during secondary processes.

6.4. Composition of sources and melting processes

6.4.1. Al-depletion and garnet fractionation

Globally two main geochemical types of komatiites are distinguished by their major element contents (Nesbitt and Sun, 1976; Sun, 1984), notably their Al content. More recently Arndt (2003) has classified the komatiites as Al-depleted Barberton-type and Al-undepleted Munro-type. The Barberton-type komatiites are most common in the oldest (>3.3 Ga) Archaean greenstone belts, whereas the Munro-type komatiites are characteristic of late Archaean (~2.7 Ga) greenstone belts and also found in Proterozoic and younger regions such as Gorgona island (Kerr et al., 1996). The compositions of both types of komatiites are interpreted to reflect melting of essentially anhydrous but unusually hot mantle sources (Arndt et al., 1998; Herzberg, 1992). The Al-depleted Barberton-type komatiites are attributed to melting in the presence of garnet. At low pressure, garnet melts near the peridotite solidus and is eliminated from the residue before the melt acquires an ultramafic composition (Arndt, 2003). For garnet to be retained in the residue of an ultramafic magma, the pressures must be high. Experimental studies (Ohtani et al., 1989; Herzberg, 1999) have shown that the major element compositions of Al-depleted Barberton-type komatiites are best explained by partial melting of garnet peridotite at pressures greater than 8 GPa. Al-undepleted Munro-type komatiites are explained to result from high degree (~50%) of peridotite melting at shallower level, where the mantle source intersected the solidus and garnet was eliminated from the residue before the melts acquired ultramafic composition. At such level the ultramafic melt is less dense than the residue (Arndt, 1994, 2003).

Many workers (e.g. Jahn et al., 1982; Gruau et al., 1992) have used CaO/Al_2O_3 ratios in combination with $(Gd/Yb)_N$ values to constrain source characteristics, particularly garnet fractionation or retention in the source, where high CaO/Al_2O_3 ratios (>1.0) and $(Gd/Yb)_N$ values (>1.0) are attributed to varying degree of garnet involvement in the source as residual phase, while low CaO/Al_2O_3 ratios (<1.0) and $(Gd/Yb)_N$ values (<1.0) could be attributed to garnet entering into the melt phase.

About two thirds of the analysed samples are characterised by Al-depletion with high CaO/Al_2O_3 (>1.0) and Al_2O_3/TiO_2 (<16) implying involvement of garnet as residual phase, while the remaining samples are Al-undepleted with CaO/Al_2O_3 (<1.0) and Al_2O_3/TiO_2 (18–24), indicating dissolution of garnet/garnet entering into the melt. Komatiites samples with high MgO contents (>30 wt.%) generally display CaO/Al_2O_3 ratios >1.0, whereas samples with lower MgO contents (<30 wt.%) have CaO/Al_2O_3 ratios <1.0. Chikhaoui (1981) has shown that the Ca content in volcanic rocks is generally reduced by hydrous alteration; hence the CaO/Al_2O_3 ratios are expected to be lowered. This could explain the low CaO/Al_2O_3 ratios observed in few samples despite high MgO and low Al_2O_3/TiO_2 ratios. Major element ratios such as CaO/Al_2O_3 and Al_2O_3/TiO_2 in combination with $(Gd/Yb)_N$ values have been used to constrain the nature of mantle sources and garnet fractionation (Jahn et al., 1982; Arndt, 2003). In the present study bivariate plots of $(Gd/Yb)_N$ versus CaO/Al_2O_3 (Fig. 12) and Al_2O_3/TiO_2 (Fig. 13) suggest varying degree of garnet involvement either as residual phase in the source or garnet entering into the melt phase.

6.4.2. Depth of magma generation and temperatures of eruption

The geochemical characteristics [high MgO, Ni, Cr and $(Gd/Yb)_N > 1$] of Al-depleted komatiites suggest that garnet

(majorite?) remained (largely) in the residue during melting process implying a derivation of komatiite magmas from great depths (about 400 km). Those samples with lower CaO/Al_2O_3 (<1.0) and higher Al_2O_3/TiO_2 (>16) ratios and slightly higher Zr, Hf and Y compared to primitive mantle might have been generated at shallower depth (about 250–300 km) without involvement of residual garnet. The MgO vs FeO diagram of Hanson and Langmuir (1978) is used to constrain the liquidus temperature and degree of melting, and also to evaluate the relationship between the peridotitic komatiites and komatiitic basalts. Our data projected on this diagram (figure is not given) show that only peridotitic komatiites plot within the field of liquids that could have co-existed with upper mantle peridotite. These komatiites were generated by high degrees of melting with initial melt temperatures as high as 1600 °C.

6.4.3. Constraints from trace elements

The majority of komatiites studied displays chondritic to sub-chondritic REE patterns indicating their derivation from a depleted mantle source. REE modelling indicates 15–30% melting of the mantle source at different depths with garnet (0–15%) in residue account most of the observed REE contents except two samples (KL-2 and NH-1) which show higher REE contents (10–20 times of chondrites). The latter two samples could represent either late fractionates or result from very low degree melting as they contain mainly clinopyroxene and/or its

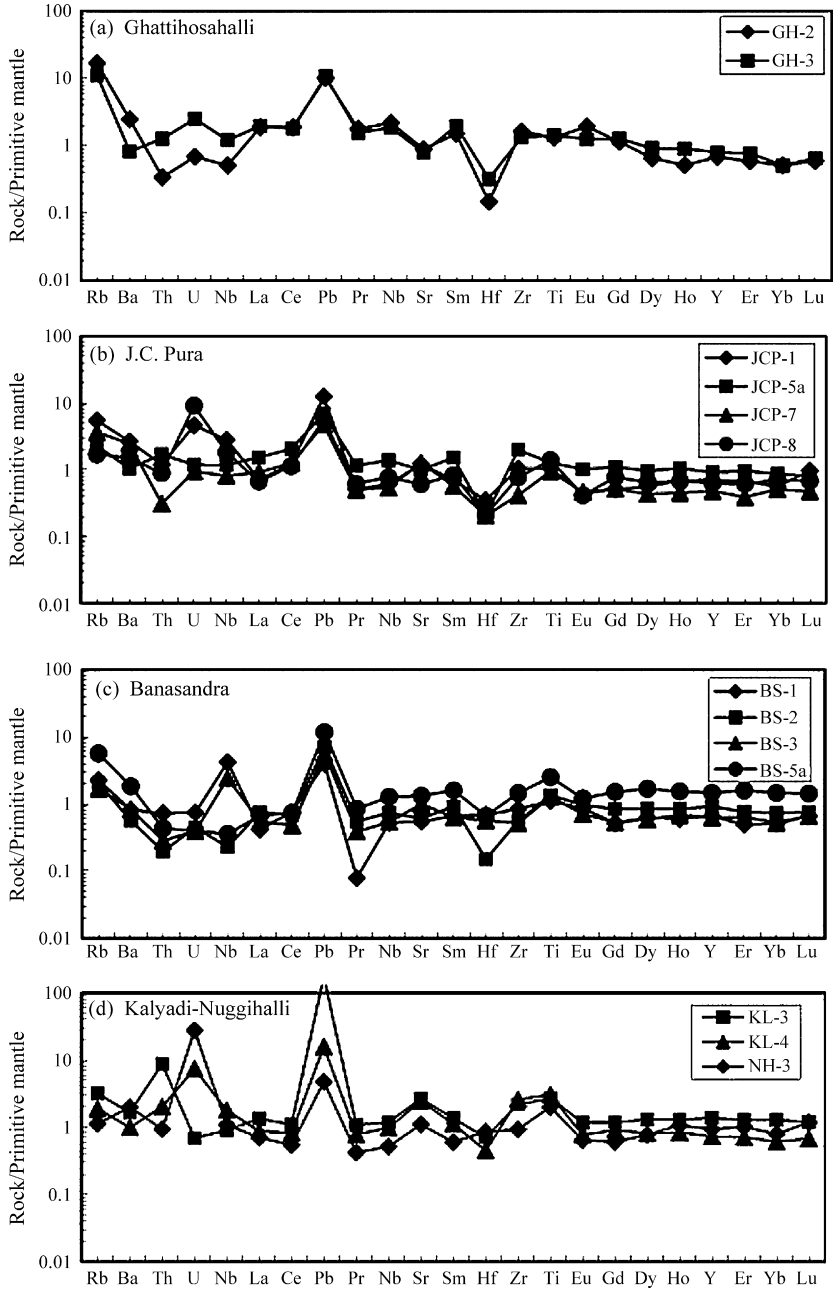

Fig. 11. (a–c) Primitive mantle (Hoffman, 1988) normalized multielement diagrams of Ghattihosahalli, J.C. Pura and Banasandra Komatiites. (d–f) Primitive mantle (Hoffman, 1988) normalized multielement diagrams of Kalyadi–Nuggihalli komatiites.

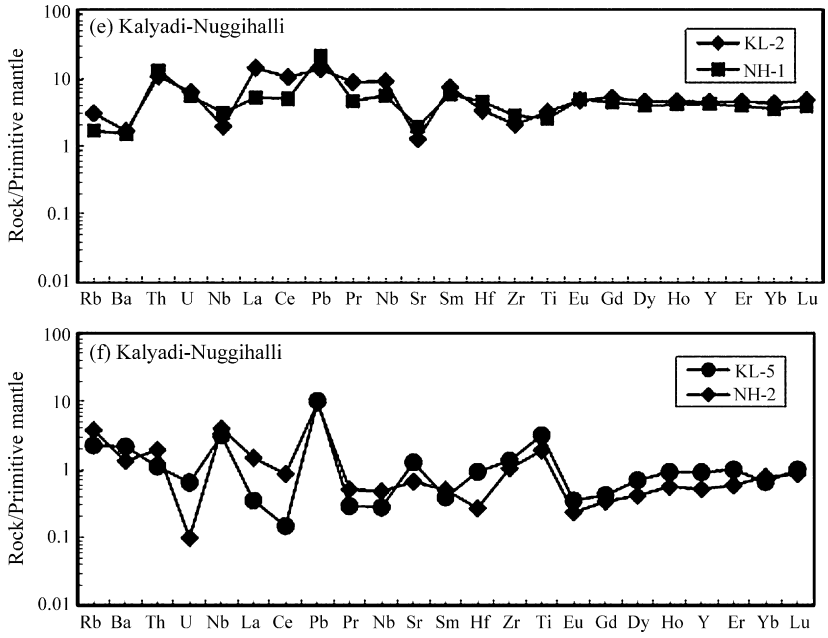

Fig. 11. (*Continued*).

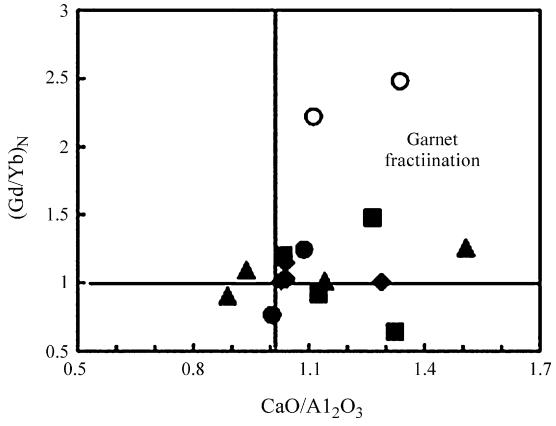

Fig. 12. $(Gd/Yb)_N$ ratios vs. CaO/Al_2O_3 plot for the komatiites of the WDC.

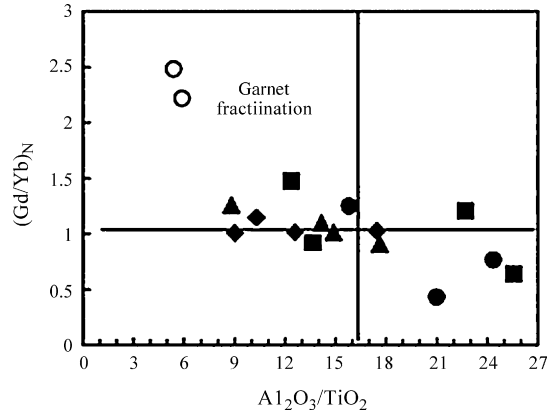

Fig. 13. $(Gd/Yb)_N$ ratios vs. Al_2O_3/TiO_2 plot for the komatiites of the WDC.

metamorphic products (actinolite, tremolite with sub-ordinate hornblende). Zr, Hf and Y anomalies have been used to constrain the nature of sources and melt residues (Fan and Kerrich, 1997). About two-third of the samples exhibit moderate to strong negative Hf anomalies in primitive mantle-normalized spider diagrams (see Fig. 11a–f), which implies their derivation from a deep mantle source where garnet fractionated or was retained in the residue (cf. Fan and Kerrich, 1997). The remaining samples show flat HREE with no or slight positive Hf and Zr anomalies, which could be attributed to their derivation from a shallower mantle source with garnet behaving as a non-residual phase.

Nb-anomalies on primitive mantle-normalised multi-element diagrams are used to identify different mantle sources and mechanisms of magma generation (cf. Jochum et al., 1991). Negative Nb-anomalies have been attributed to shallow mantle sources in arc environments or to crustal contamination, while positive Nb-anomalies have been explained by magma derivation from a deep complementary reservoir of arc magmatism (Polat and Kerrich, 2000). Positive Nb-anomalies in Archaean komatiites-basalts have been attributed to their derivation from a plume source that contains slab material recycled to deepest mantle levels (Kerrich and Xie, 2002). On the other hand, the time required for deep recycling of Archaean slab into plume is not well constrained, but recycling rates of slabs are considered to be faster during the Archaean (Fyfe, 1978). For the majority of studied samples positive or lacking Nb-anomalies on the primitive mantle-normalised multi-element diagrams imply a deep mantle plume source probably containing recycled slab component (Kerrich and Xie, 2002). Those samples displaying slight negative Nb-anomalies coupled with absent Hf anomalies may have been derived from a shallower mantle source with garnet melting or elimination of garnet from the residue before the melt acquired ultramafic composition (cf. Arndt, 2003). Alternatively, inter-

action of deep mantle-derived magmas with continental crust could explain the observed slight negative Nb-anomalies and zero Hf anomalies. However, low SiO_2, high MgO, Ni and Cr coupled with low LREE contents do not correlate with the magnitude of Nb-anomalies. McCuig et al. (1994) have modelled the HFSE/REE fractionation resulting from pyrope and majorite garnet retention during melting of primitive mantle. Retention of majorite garnet results in more pronounced Zr and Hf anomalies than pyrope retention. Given the negative Hf anomalies and corresponding $(Gd/Yb)_N$ values, the lower HREE and Y concentrations compared to primitive mantle in the Al-depleted komatiites, would imply melt segregation in the deeper mantle with possible garnet (majorite?) retention in the source. Majorite garnet stability in mantle peridotite signifies pressures of at least 14 GPa, corresponding to depths of at least 400 km (Miller et al., 1991; Herzberg, 1999; Xie et al., 1993; Fan and Kerrich, 1997). On the other hand, komatiite samples with low $(Gd/Yb)_N$ values (<1.0) and absence of Hf anomalies could be interpreted by melting of shallower mantle without involvement of garnet in the residue. Consequently the observed range of $(Gd/Yb)_N$ values coupled with absence of negative Hf anomalies, higher Y, Zr and HREE concentrations could be interpreted by generation of komatiite magmas at different depths either with or without involvement of garnet.

6.4.4. Constraints from Nd isotopes

The large Sm/Nd spread and the range of Nd isotope compositions measured (Table 1) on the west Dharwar komatiites allow to define a relatively precise whole-rock isochron (see Fig. 5). However, out of 20 samples analysed, 16 samples define an isochron whilst four samples plot outside the main trend, which could be related to alteration of their Sm/Nd ratios during secondary processes associated with greenschist- to lower amphibolite facies metamorphism. Three samples display very high positive $\varepsilon_{Nd}(t)$ values (+5.0 to +7.4) and plot above the isochron; this may be related to either derivation from strongly depleted mantle sources or secondary alteration of their Sm/Nd ratios. REE and other incompatible element contents of those three samples do not indicate highly depleted mantle sources. Consequently their anomalous positive $\varepsilon_{Nd}(t)$ values may be attributed to secondary processes. The sample that exhibit negative $\varepsilon_{Nd}(t)$ value (−2.5) and plot below the isochron despite being depleted in LREE might have been affected by secondary fluid induced processes during metamorphism. The 16 samples reported on the isochron show ε_{Nd} values ranging between +0.5 to +2.9 at 3352 Ma, values which indicate a derivation of komatiites from a depleted mantle at 3.35 Ga.

6.5. Middle Archaean crustal growth, mantle evolution and geodynamic settings in the Western Dharwar Craton

6.5.1. Middle Archaean greenstone volcanism, TTG accretion and mantle evolution

The present study indicates a phase of widespread komatiite volcanism in the Sargur Group greenstone basins of the Western Dharwar Craton close to 3352 Ma. This event caused a significant addition of new crust. Published isotopic age data also indicate sub-contemporaneous accretion of TTG-type Peninsular gneisses during middle Archaean.

Several studies (O'Nions et al., 1979; De Paolo, 1980; Patchett et al., 1981; Allegre et al., 1983; Stein and Hofmann, 1994) suggested a spatial link between the evolution of mantle reservoirs and formation of continental crust. More recently, Boyet and Carlson (2005) based on $^{142}Nd/^{144}Nd$ isotope data argued that depleted mantle reservoirs evolved very early in the Earth's history during 4.53 Ga global differentiation of silicate Earth, and that complimentary enriched reservoir probably located at the base of the mantle never have been sampled. In the estimation of depleted mantle compositions a large proportion of the data are from komatiites, and the assumption is made that the source of these rocks is equivalent to modern depleted upper mantle. The problems associated with alteration and crustal contamination of komatiites constitutes a major limitation in characterising the mantle. If komatiites form by deep melting of the conduits of mantle plumes, their sources will be quite different from the Archaean upper mantle. Consequently, Archaean komatiites derived from deep mantle plume sources (>400 km) are not suitable to characterise the evolution of the upper mantle. Several recent studies (Grove et al., 1999; Parman et al., 1997, 2001; Puchtel et al., 1999) argue that komatiite magmas can be derived from the upper mantle in an arc environment and thus can be used for characterising the depletion of the upper mantle.

In WDC the lithospheric mantle was depleted in incompatible elements as a consequence of the extraction of crustal protoliths of the 3400 Ma Gorur-type gneisses and provenance of 3580 Ma sediments. Komatiite magmas that formed at greater depths also show depletion, which can be attributed to their sources having already been depleted in earlier melting event(s), probably an earlier plume-related greenstone volcanism. Thus, it may be speculated that the mantle source of the komatiites has lost incompatible elements through extraction of a melt component during an earlier (∼3600 Ma?) plume related greenstone volcanism.

The positive ε_{Nd} values +0.5 to +2.9 at 3352 Ma (excluding anomalous values) of komatiites suggest their derivation from a depleted mantle which experienced a long term depletion history. The existence of such depleted mantle reservoirs at 3352 Ma indicates extraction of crust from the mantle prior to komatiite volcanism at 3352 Ma which in turn implies significant crustal growth during early Archaean to middle Archaean in the WDC.

6.5.2. Geodynamic setting

The geodynamic context of komatiite magma generation and eruption is still a matter of debate, as whether they are related to mantle plume (Ohtani et al., 1989; Arndt et al., 1997; Arndt, 2003; Kerrich and Xie, 2002), an oceanic plateau originated from mantle plume (Kerr et al., 1996; Polat and Kerrich, 2000), a combined mantle plume-island arc environment (Puchtel et al., 1999) or a subduction zone (Parman et al., 1997, 2001; Grove et al., 1999).

In the Western Dharwar Craton, both uniformitarian models involving an arc setting (Drury, 1983; Krogstad et al., 1989;

Newton, 1990; Chadwick et al., 2000; Manikyamba et al., 2004, 2005) and non-uniformitarian models involving vertical accretion in hot spot environments associated with rising plumes (Choukroune et al., 1995, 1997) have been proposed to explain greenstone volcanism and TTG accretion.

Any geodynamic model proposed for 3352 Ma komatiite volcanism in the WDC must account for sub-contemporaneous mafic to felsic volcanism in the greenstone belts and the surrounding TTG basement. In order to account for the observed age relationships of komatiites with the associated mafic/felsic volcanics and surrounding TTG basement several models have been considered.

6.5.3. Subduction zone setting

Lateral accretion of crust in the subduction zone context is considered as a major process in the origin of Archaean cratons (for review see Martin and Moyen, 2002; Smithies et al., 2003). During early to middle Archaean geothermal gradients were much higher than in the modern Earth (Martin, 1986). This model is often proposed for the formation of continental crust of TTG composition and in large part accounts for the general andesitic composition of the Archaean continental crust (Taylor and McLennan, 1985). For the Western Dharwar Craton, Drury (1983) proposed an arc setting to explain the origin of mafic volcanics. More recently, Parman et al. (1997, 2001) proposed a subduction zone setting for the 3.45 Ga Barberton komatiites. However, this model has been widely debated (for review see Arndt, 2003; Chavagnac, 2004) as it cannot account for the chemical characteristics (particularly Al-depletion, positive or lacking Nb anomalies, Nb/U, Nb/Th, Nb/La, Th/U ratios) of the komatiites and also their high eruption temperatures (∼1600 °C). Consequently the observed geochemical characteristics (high MgO, Al-depletion, Nb, Zr, Hf, Y and HREE) of komatiites are not consistent with an arc environment.

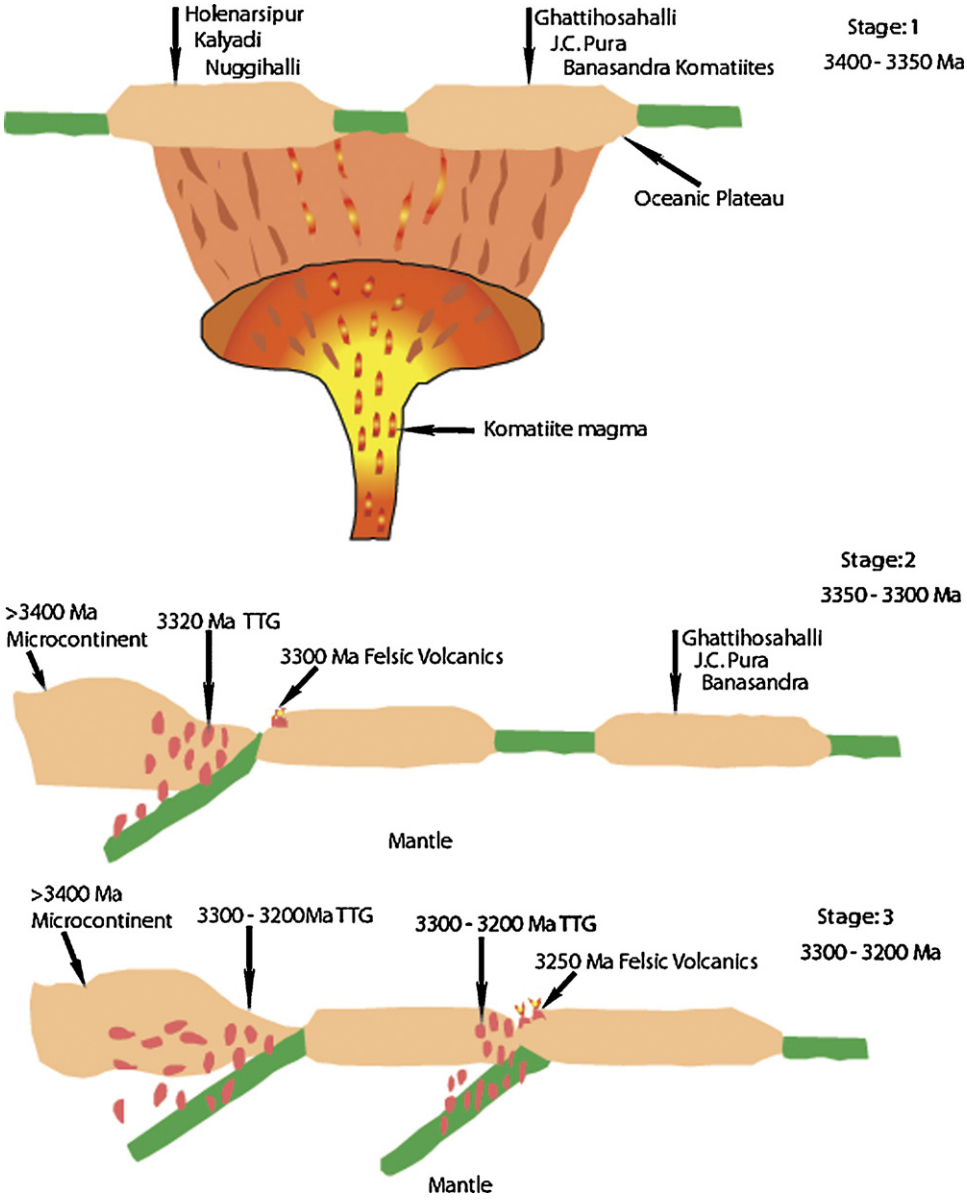

Fig. 14. Cartoon showing plume-arc model for the formation of komatiites and sub-contemporaneous mafic/felsic volcanics and TTG in the WDC.

6.5.4. Plume model

Many workers have presented a different model based on geochemical constraints of ultramafic rocks in Archaean greenstone belts. The high magnesium, Al-depletion, low incompatible element contents together with their high eruption temperatures (1600–1700 °C) led to the consideration that these ultramafic rocks reflect a high degree of melting of mantle at great depths, in the hottest portion of ascending mantle plumes (Campbell et al., 1989; Ohtani et al., 1989; Griffith and Campbell, 1992; Arndt et al., 1997; Arndt, 1994, 2003; Chavagnac, 2004).

The majority of studied komatiites show high contents of MgO, Ni and Cr, Al-depletion, absent or positive Nb anomalies, negative Hf anomalies consistent with their generation in a deep mantle hot spot environment associated with a rising plume. Thus geochemical characteristics together with high melt temperatures and great depth of melt generation of the studied komatiites argue in favour of plume setting for their origin. However, the plume model alone does not account for the geochemical characteristics contemporaneous felsic volcanics and sub-contemporaneous TTG basement.

6.5.5. Plume-arc model

The lithological frame work of the Sargur Group greenstone belts and surrounding TTG basement and their age relationships together with geochemical characteristics require distinct geodynamic settings: (1) the TTG gneiss basement constitutes a complex of 3.32–3.23 Ga continental crust which appears to have formed by melting of oceanic slab in an arc environment (Martin, 1986), (2) the plume-derived komatiite volcanic complexes represent remnants of oceanic plateau, and (3) the mafic–felsic volcanics subduction-related rocks, which intrude and overlie the oceanic plateau.

The isotopic and geochemical data of the ultramafic rocks strongly suggest that no older felsic crust was involved in their petrogenesis. This implies that the mantle plume was initiated beneath an oceanic crust away from any sizable ancient continental mass leading to formation of oceanic plateau (Fig. 14). The ultramafic sequences in the Western Dharwar Craton contain abundant pillow lavas that unambiguously point to their eruption in a marine environment. Isotopic age data (Peucat et al., 1995; this study) indicate that the time span between the formation of this oceanic plateau and that of the subduction zone related mafic–felsic volcanic complex was about 50 Ma. Abbott et al. (1994) estimated that a plume has the thermal potential to produce a komatiitic to basaltic oceanic plateau with an average thickness of ~35 km. Oceanic plateaus of such thickness are typically underlain by refractory lithospheric mantle roots buoyant enough to resist subduction (Abbot and Mooney, 1995; Cloos, 1993). Rapid subduction of intervening hot oceanic crust in back-arc environments generates mafic/felsic magmas at different depths. These magmas intrude the oceanic plateau and thus erupt in a subduction zone environment (see Fig. 14). Magmas generated in such arc environment crystallise in deep levels as protoliths of TTG. Consequently, a plume-arc model can account for most of the observed characteristics including the close spatial association and sub-contemporaneous nature of middle Archaean Sargur Group greenstones-TTG basement in the WDC.

7. Conclusions

The conclusions of the present study can be summarised as follows:

1. Widespread 3.35 Ga komatiite volcanism in the Western Dharwar Craton is sub-contemporaneous with granitoid plutonism of the surrounding TTG-basement.
2. Komatiite magmas were derived by melting of upper mantle at different depths (about 400 km or less) with or without garnet (majorite?) in the residue.
3. Komatiite magmas co-existed with mantle peridotite with solidus temperatures as high as 1600 °C.
4. Trace element characteristics together with Nd isotope data suggest that the komatiites were derived from a depleted mantle source.
5. The existence of a depleted mantle reservoir at 3.35 Ga implies that the upper mantle had already lost a melt component during the early Archaean (>3.6 Ga) crustal growth through a preceeding greenstone-TTG cycle.
6. The komatiite volcanism and associated sub-contemporaneous mafic to felsic volcanism and granitoid plutonism in the surrounding TTG basement can be best explained by a plume-arc model.

Acknowledgements

This work was funded by Japanese Society for Promotion of Science (JSPS) collaborative Grant-in-Aid research grant 14540427. We thank S.V. Srikantia, H.S.M. Prakash, D.N. Subramanyam, and N. Mahesh for their help during the course of this work. Nicole Morin thanked for her help in Nd isotope analysis. We thank Prof. M. Raith and Prof. Somnath Dasgupta for inviting to contribute the paper, for editorial support and patience with the submission of the revised manuscript. Constructive reviews by H.G. Stoch and Y.J. Bhaskar Rao greatly helped to improve the quality of the paper.

Appendix A. Analytical methods

Samples were crushed at the Department of Geology, Bangalore University with agate mill. Powdered rock specimens were fused into homogeneous glass beads with a mixed alkali flux ($Li_2B_4O_7$, Spectromelt A10, Merck). Major elements and selected trace elements (Rb, Ba, Ni, Cr, Co, V) were analyzed by XRF (Rigaku RIX 3000) at centre for instrumentation centre, Yamaguchi University (Japan). The calibration curves for each element were based on 15 international reference standard samples (JB-1a, JB-2, JB-3, JA-1, JA-2m, JA-3, JG-1a, JG-2, JG-3, JR-1, JR-2, JGb-1, JP-1, JF-1 and JF-2) of the Geological Survey of Japan. The analytical values were checked by repeated analyses of JG-1a and JB-1a in every 10 analyses of unknown. For trace elements, precision is better than 5%; for contents less than 30 ppm the uncertainties are within 10% and for those elements

with concentration less than 5 ppm uncertainty in the range of 10–50%.

Other trace elements including REE were analyzed by using ICP-MS (Fisons Instruments Plasma Quad PQ 111, U.K.) at Curtin University of Technology, Perth, Western Australia. Samples for ICP-MS analysis were prepared by dissolving 0.5 g powder using HF, HNO_3, $HClO_4$ and HCl. Quantification is achieved with reference to in house standards SY2, SARM2, SARM3, SARM4 for REE and NIM D, NIM G, SARM50 for Nb, U, Th and Hf. Nd isotope compositions for whole-rocks were determined using a Finnigan Mat 262 mass spectrometer at Geosciences Rennes. Total blanks for Sm and Nd contents were lower than 0.05 ng. Uncertainties are 0.2% for $^{147}Sm/^{144}Nd$ ratios. Replicate analyses of La Jolla standard yield a mean $^{143}Nd/^{144}Nd$ ratio of 0.511857 ± 3. Two set of Nd_{DM} model ages are calculated in Table 1, for samples having negative ε_0 values, with two different DM ($\varepsilon_0 = +8$ by Nagler et al., 1998; +9.5 by De Paolo, 1980) and a $^{147}Sm/^{144}Nd$ ratio of 0.2137, assuming a radiogenic linear growth for the mantle starting at 4.54 Ga, following De Paolo (1981). Isochron age was calculated using Isoplot 2.49 software of Ludwig (2001).

References

Abbot, D., Mooney, W., 1995. The structural and geochemical evolution of the continental crust: support for the oceanic plateau model of continental growth. Rev. Geophys. Suppl., 231–242.

Abbott, D.H., Burgess, L., Longhi, J., Smith, W.H.F., 1994. An empirical thermal history of the earth's upper mantle. J. Geophys. Res. 99, 13835–13850.

Allegre, C.J., Hart, S.R., Minster, J.F., 1983. Chemical structure and evolution of the mantle and continents determined by inversion of Nd and Sr isotopic data. I. Theoretical methods. Earth Planet. Sci. Lett. 66, 177–190.

Anil Kumar, Bhaskar Rao, Y.J., Sivaraman, T.V., Gopalan, K., 1996. Sm–Nd ages of Archaean metavolcanics of the Dharwar craton, south India. Precambrian Res. 80, 205–216.

Arndt, N.T., 1994. Archaean komatiites. In: Condie, K.C. (Ed.), Archaean Crustal Evolution. Elsevier, Amsterdam, pp. 11–44.

Arndt, N.T., 2003. Komatiites, kimberlites and boniites. J. Geophys. Res. 108 (B6), 2293, doi:10.1029/2002JB002157.

Arndt, N.T., Nisbet, E.G., 1982. Komatiites. George Allen and Unwin Publ., UK.

Arndt, N.T., Kerr, A.C., Tarney, J., 1997. Dynamic melting in plume heads: the formation of Gorgana komatiites and basalts. Earth Planet. Sci. Lett. 146, 289–301.

Arndt, N.T., Albarede, M.M., Cheadle, C., Ginibre, C., Herzberg, G., Jenner, C., Chauvel, C., Lahaye, Y., 1998. Were komatiites wet? Geology 26, 739–742.

Balakrishnan, S., Hanson, G.N., Rajamani, V., 1990. Pb and Nd isotope constraints on the origin of high Mg and tholeiitic amphibolites, Kolar Schist Belt, South India. Contrib. Mineral. Petrol. 107, 272–292.

Balakrishnan, S., Rajamani, V., Hanson, G.N., 1999. U–Pb ages for zircon and titanite from the Ramagiri area, southern India: evidence for accretionary origin of the eastern Dharwar craton during the late Archaean. J. Geol. 107, 69–86.

Bhaskar Rao, Y.J., Sivaraman, T.V., Pantulu, C.V.C., Gopalan, K., Naqvi, S.M., 1992. Rb–Sr ages of late Archaean metavolcanics and granites, Dharwar craton, south India and evidence for early Proterozoic thermotectonic event(s). Precambrian Res. 59, 145–170.

Bhaskar Rao, Y.J., Anil Kumar, Vrevsky, A.B., Srinivasan, R., Anantha Iyer, G.V., 2000. Sm–Nd ages of two meta-anorthosite complexes around Holenarsipur: constraints on the antiquity of Archaean supracrustal rocks of the Dharwar craton. Proc. Ind. Acad. Sci. (Earth Planet. Sci.) 109, 57–66.

Boyet, M., Carlson, R.W., 2005. ^{142}Nd evidence for early (>4.53 Ga) global differentiation of silicate Earth. Science 309, 577–581.

Braun, J.J., Pagel, M., Herbillon, A., Rosin, C., 1993. Mobilization and redistribution of REEs and thorium in a syenitic lateritic profile: a mass balance study. Geochim. Cosmochim. Acta 57, 4419–4434.

Campbell, I.H., Griffiths, R.W., Hill, R.I., 1989. Melting in an Archean mantle plume: head its basalts and tail its komatiites. Nature 339, 697–699.

Chadwick, B., Vasudev, V.N., Hegde, G.V., 2000. The Dharwar craton, southern India, interpreted as the result of Late Archaean oblique convergence. Precambrian Res. 99, 91–111.

Charan, S.N., Naqvi, S.M., Ramesh, S.L., 1988. Geology and geochemistry of spinifex-textured peridotitic komatiite from Mayasandra Schist Belt. J. Geol. Soc. India 32, 343–350.

Chardon, D., 1997. Les deformations continental archeenes, examples at modelisation thermomechanique. Memoire Geosciences-Rennes 76, 300 p.

Chardon, D., Peucat, J.-J., Jayananda, M., Choukroune, P., Fanning, C.M., 2002. Archaen granite-greenstone tectonics at Kolar (South India): interplay of diapirism, bulk inhomogenous contraction during juvenile accretion. Tectonics 32, 1029–1047.

Chavagnac, V., 2004. A geochemical and Nd isotopic study of Barberton komatiites (South Africa): implication for the Archean mantle. Lithos 75, 253–281.

Chikhaoui, M., 1981. Les roches volcaniques du proterozoique superieur de la chaine pan-Africaine dans le NW de l' Afrique (Hoggar, Anti-Atlas, Adrar des Iforas): caracterisation geochimique et mineralogique, implications geodynamiques. These d' Etat, Montpellier, 183 p.

Choukroune, P., Bouhallier, H., Arndt, N.T., 1995. Soft lithosphere during periods of Archaean crustal growth or crustal reworking. In: Coward, M.P., Riess, A.C. (Eds.), Early Precambrian Processes, vol. 95. Geol. Soc. Spec. Publ., pp. 67–86.

Choukroune, P., Ludden, J.N., Chardon, D., Calvert, A.J., Bouhallier, H., 1997. Archaean crustal growth and tectonic processes: a comparision of the Superior Province, Canada and the Dharwar craton. In: Burg, J.-P., Ford, M. (Eds.), Orogeny Through Time, vol. 121. Geol. Soc. Spec. Publ., India, pp. 63–98.

Cloos, M., 1993. Lithospheric buoyancy and collisional orogenesis: subduction of oceanic plateaus, continental margins, island arcs. Spreading ridges, and seamounts. Geol. Soc. Am. Bull. 105, 715–737.

De Paolo, D.J., 1980. Crustal growth and mantle evolution: inferences from models of element transport and Nd and Sr isotopes. Geochim. Cosmochim. Acta 44, 1185–1196.

De Paolo, D.J., 1981. Neodymium isotopes in Colarado Front Range and crust–mantle evolution in Proterozoic. Nature 291, 193–196.

Devapriyan, G.V., Anantharamu, T.R., Vidyadharan, K.T., Raghu Nandan, K.R., 1994. Spinifex textured peridotitic komatiite from Honnabetta area, Nagamangala schist belt, Karnataka. J. Geol. Soc. India 44, 483–493.

Drury, S.A., Van Calstren, P.C., Reeves-Smith, G.J., 1987. Sm–Nd isotopic data from Archaean metavolcanic rocks at Holenarasipur, South India. J. Geol. 95, 837–843.

Drury, S.A., 1983. The petrogenesis and setting of Archaean volcanics from Karnataka state, South India. Geochim. Cosmochim. Acta 47, 317–329.

Fan, J., Kerrich, R., 1997. Geochemical characteristics of Al-depleted and undepleted komatiites and HREE-enriched tholeiites, western Abitibi greenstone belt: variable HFSE/REE systematics in a heterogeneous mantle plume. Geochim. Cosmochim. Acta 61, 4723–4744.

Fyfe, W.S., 1978. The evolution of the Earth's crust: modern plate tectonics to ancient hot spot tectonics. Chem. Geol. 23, 89–114.

Griffith, R.W., Campbell, I.H., 1992. On the dynamics of long-lived plume conduits in the convecting mantle. Earth Planet. Sci. Lett. 103, 214–227.

Grove, T.L., deWit, M.J., Dann, J., 1997. In: deWit, M.J., Ashwal, L.D. (Eds.), Komatiites from the Komati type section, Barberton, South Africa, in Greenstone Belts. Oxford Sci., Oxford, pp. 422–437.

Grove, T.L., Parman, S.W., Dann, J.C., 1999. Conditions of magma generation for Archaean komatiites from the Barberton Mountain land, South Africa. In: Fei, Y., Bertla, C.M., Mysen, B.O. (Eds.), Mantle Petrology: Field Observations and High Pressure Experimentation. The Geochemical Society, Cadmus Journal Services, Lancaster, pp. 155–167.

Gruau, G., Jahn, B.M., Glikson, A.Y., Davy, R., Hickman, A.H., Chauvel, C., 1987. Age of the Archaean Talga-Talga subgroup, Pibara Block, Western Australia, and early evolution of the mantle: new Sm–Nd isotopic evidence. Earth Planet. Sci. Lett. 85, 105–116.

Gruau, G., Toupin, S., Fourcade, S., Blais, S., 1992. Loss of (Nd, O) and chemical (REE) memory during metamorphism of komatiites: new evidence from eastern Finland. Contrib. Mineral. Petrol. 112, 66–82.

Hanson, G.N., Langmuir, C.H., 1978. Modelling of major elements in mantle-melt systems using trace element approaches. Geochim. Cosmochim. Acta 42, 725–741.

Herzberg, C., 1999. Phase equilibrium constraints on the formation of cratonic mantle. In: Fei, Y., Bertka, C.M., Mysen, B.O. (Eds.), Mantle Petrology: Field Observations and High-Pressure Experimentation, vol. 6. Spec. Publ. Geochem. Soc., pp. 241–257.

Herzberg, C.T., 1992. Depth and degree of melting of komatiites at high pressures. J. Geophys. Res. 97, 4521–4540.

Hoffman, A.W., 1988. Chemical differentiation of the Earth: the relationship between mantle, continental crust and oceanic crust. Earth Planet. Sci. Lett. 90, 297–314.

Jaffri, S.H., Subba Rao, D.V., Ahmad, S.M., Mathur, R., 1997. Spinifex textured peridotitic komatiites from Nuggihalli and Holenarsipur schist belts, Karnataka. J. Geol. Soc. India 49, 33–38.

Jahn, B.M., Gruan, G., Glikson, A.Y., 1982. Komatiites of the Onverwacht Group, South Africa. REE geochemistry, Sm/Nd age and mantle evolution. Contrib. Mineral. Petrol. 80, 25–40.

Jayananda, M., Peucat, J.-J., 1996. In: Santosh, M., Yoshida, M. (Eds.), Geochronological framework of Southern India: The Archaean and Proterozoic terrains of Southern India within East Gondwana, vol. 3. Gondwana Research Group Memoir, pp. 53–75.

Jayananda, M., Moyen, J.-F., Martin, H., Peucat, J.-J., Auvray, B., Mahabaleswar, B., 2000. Late Archean (2550–2520 Ma) juvenile Magmatism in the Eastern Dharwar craton, southern India: constraints from geochronology, Nd–Sr isotopes and whole rock geochemistry. Precambrian Res. 99, 225–254.

Jayananda, M., Chardon, D., Peucat, J.-J., Capdevila, R., 2006. 2.61 Ga potassic granites and crustal reworking in the western Dharwar craton, southern India: tectonic, geochronologic and geochemical constraints. Precambrian Res. 150, 1–26.

Jensen, L.S., 1976. A new method of classifying alkali volcanic rocks. Ont. Div. Min., Misc. Paper 66, 22 p.

Jochum, K.P., Arndt, N.T., Hofmann, A.W., 1991. Nb–Th–La in komatiites and basalts: constraints on komatiites petrogenesis and mantle evolution. Earth Planet. Sci. Lett. 107, 272–289.

Kerr, A.C., Marriner, G.F., Arndt, N.T., Tarney, J., Nivia, A., Saunders, A.D., Duncan, R., 1996. The petrogenesis of Gorgona komatiites, picrites and basalts: new field, petrographic and geochemical constraints. Lithos 37, 245–260.

Kerrich, R., Wyman, D., Hollings, P., Polat, A., 1999. Variability of Nb/Th and Th/La in 3.0 to 2.7 Ga Superior province ocean plateau basalts: implications for the timing of continental growth and lithosphere recycling. Earth Planet. Sci. Lett. 168, 101–115.

Kerrich, R., Xie, Q., 2002. Compositional recycling structure of an Archaean super-plume: Nb–Th–U–LREE systematics of Archaean Komatiites and basalts revisited. Contrib. Mineral. Petrol. 142, 476–484.

Krogstad, E.J., Hanson, G.N., Rajamani, V., 1991. U–Pb ages of zircon and sphene for two gneiss terranes adjacent to the Kolar schist belt, south India: evidence for separate crustal evolution histories. J. Geol. 99, 801–816.

Krogstad, E.J., Balakrishnan, S., Mukhopadhyaya, D.K., Rajamani, V., Hanson, G.N., 1989. Plate tectonics at 2.5 by ago: evidence from Kolar schist belt, South India. Science 243, 1337–1340.

Lahaye, X., Arndt, N.T., Byerly, G., Chauvel, C., Fourcade, S., Gruau, G., 1995. The influence of alteration on the trace-element and Nd isotopic compositions of Komatiites. Chem. Geol. 126, 43–64.

Lecuyer, C., Gruau, G., Anhaeusser, C.R., Fourcade, S., 1994. The origin of fluids and the effect of metamorphism on the primary chemical compositions of Barberton komatiites; new evidence from geochemical (REE) and isotopic (Nd, O, H, $^{39}Ar/^{40}Ar$) data. Geochim. Cosmochim. Acta 58, 969–984.

Lesher, C.M., Arndt, N.T., 1995. REE and Nd isotope geochemistry, petrogenesis and volcanic evolution of contaminated komatiites at Kambalda, vol. 34. Lithos, Western Australia, pp. 127–157.

Ludden, J.N., Gelinas, L., Trudel, P., 1982. Archaean metavolcanics from the Rouyn-Noranda district, Abitibi greenstone belt, Quebec. 2. Mobility of trace elements and petrogenetic constraints. Can. J. Earth Sci. 19, 2276–2287.

Ludwig, K.R., 2001. Users Manual for Isoplot/Ex. Rev.2.49. A Geochronological Tool Kit for Microsoft Excel. Berkely Geochronology Centre Special Publication. No. 1a. 2455. Ridge Road, Berkely, CA 94709, USA.

Manikyamba, C., Kerrich, R., Naqvi, S.M., Ram Mohan, M., 2004. Geochemical systematics of tholeiitic basalts from the 2.7 Ga Ramagiri-Hungund greenstone belts, Dhawar craton. Precambrian Res. 134, 21–39.

Manikyamba, C., Naqvi, S.M., Subba Rao, D.V., Ram Mohan, M., Tarun, C., Khanna, Rao, T.G., Reddy, G.L.N., 2005. Boninite from the Neoarchaean Gadwal Greenstone belt, Eastern Dharwar Craton, India: implications for Archaean subduction processes. Earth Planet. Sci. Lett. 230, 65–83.

Martin, H., 1986. The effects of steeper Archaean geothermal gradients on geochemistry of subduction zone magmas. Geology 14, 753–756.

Martin, H., Moyen, J.F., 2002. Secular changes in tonalite-trondhjemite granodiorite composition as markers of the progressive cooling of earth. Geology 30 (4), 319–322.

McCuig, T.C., Kerrich, R., Xie, Q., 1994. Phosphorus and high field strength element anomalies in Archaean high-magnesian magmas as possible indicators of source mineralogy and depth. Earth Planet. Sci. Lett. 124, 221–239.

Meen, J.K., Rogers, J.J.W., Fullagar, P.D., 1992. Lead isotopic composition in the western Dharwar craton, southern India: evidence for distinct middle Archaean terraines in a late Archaean craton. Geochim. Cosmochim. Acta 56, 2455–2470.

Miller, G.H., Stolper, E.M., Ahrens, T.J., 1991. The equation of state of molten komatiite. 2. Application to komatiite petrogenesis and the Hadean mantle. J. Geophys. Res. 96, 11849–11864.

Moyen, J.-F., Martin, H., Jayananda, M., Auvray, B., 2003. Late Archaean granites: a typology based on the Dharwar Craton (India). Precambrian Res. 127, 103–123.

Nagler, Th.F., Krammers, J.D., 1998. Nd isotopic evolution of upper mantle during Precambrian: models, data and unceratinity of both. Precambrian Res. 91, 233–252.

Naqvi, S.M., 1981. The oldest supracrustals of the Dharwar craton, India. J. Geol. Soc. India 22, 458–469.

Naqvi, S.M., Manikyamba, C., Gnaneswar Rao, T., Subba Rao, D.V., Ra Mohan, M., Srinivasa, Sarma, 2002. Geochemical and isotopic constraints of Neoarchaean fossil plume for evolution of volcanic rocks of Sandur greenstone belt, India. J. Geol. Soc. India 60, 27–56.

Nesbitt, R.W., Sun, S.S., 1976. Geochemistry of Archaean spinifex textured peridotites and magnesian low-magnesian tholeiites. Earth. Planet. Sci. Lett. 31, 433–453.

Newton, R.C., 1990. The late Archaean high grade terrain of South India and deep structure of the Dharwar craton. In: Salisbury, M.H., Fountain, D.M. (Eds.), Exposed Cross Sections of the Continental Crust. Kluwer Academic, Amsterdam, pp. 305–326.

Nutman, A.P., Chadwick, B., Krishna Rao, B., Vasudev, V.N., 1996. SHRIMP U–Pb zircon ages of acid volcanic rocks in the Chitradurga and Sandur Groups and granites adjacent to Sandur schist belt. J. Geol. Soc. India 47, 153–161.

Nutman, A.P., Chadwick, B., Ramakrishnan, M., Viswanatha, M.N., 1992. SHRIMP U–Pb ages of detrital zircon in Sargur supracrustal rocks in western Karnataka, southern India. J. Geol. Soc. India 39, 367–374.

Ohtani, E., Kawabe, I., Moriyama, J., Nagata, Y., 1989. Partitioning of elements between majorite garnet and melt and implications for petrogenesis of komatiites. Contrib. Mineral. Petrol. 103, 263–269.

O'Nions, R.K., Carter, S.R., Evensen, N.M., Hamilton, P.J., 1979. Geochemical and cosmochemical applications of Nd isotope analysis. Ann. Rev. Earth Planet. Sci. 7, 11–58.

Paranthaman, S., 2005. Geology and Geochemistry of Archaean Ghattihosahalli mafic-ultramafic complex, Chitradurga, Karnataka. J. Geol. Soc. India 66, 653–657.

Parman, S.W., Dann, J.C., Grove, T.L., de Wit, M.J., 1997. Emplacement conditions of komatiite magmas from the 3.49 Ga Komati Formation, Barberton greenstone belt, South Africa. Earth Planet. Sci. Lett. 150, 303–323.

Parman, S.W., Grove, T.L., Dann, J.C., 2001. The production of Barberton komatiites in an Archaean subduction zone. Geophys. Res. Lett. 28, 2513–2516.

Patchett, P.J., Kouvo, O., Hedge, C.E., Tatsumoto, M., 1981. Evolution of continental crust and mantle heterogeneity: evidence from Hf isotopes. Contrib. Mineral. Petrol. 78, 279–297.

Peucat, J.-J., Mahabaleshwar, B., Jayananda, M., 1993. Age of younger tonalitic Magmatism and granulite metamorphism in the south Indian transition zone (Krishnagiri area): comparison with older peninsular gneisses from Hassan-Gorur area. J. Metamorph. Geol. 11, 879–888.

Peucat, J.-J., Bouhallier, H., Fanning, C.M., Jayananda, M., 1995. Age of Holenarsipur schist belt, relationships with the surrounding gneisses (Karnataka, south India). J. Geol. 103, 701–710.

Polat, A., Kerrich, R., 2000. Archaean greenstone belt magmatism and the continental growth-mantle evolution connection: constraints from Th–U–Nb–LREE systematics of the 2.7 Ga Wawa subprovince, Superior province, Canada. Earth Planet. Sci. Lett. 175, 41–54.

Polat, A., Kerrich, R., Wyman, D.A., 1999. Geochemical diversity in oceanic komatiites and basalts from the late Archean Wawa greenstone belts, Superior Province, Canada: trace element and Nd isotope evidence for a heterogeneous mantle. Precambrian Res. 94, 139–173.

Puchtel, I.S., Hofmann, A.W., Amelin, Y.V., Garbe-Schonberg, C.D., Samsonov, A.V., Shchipansky, A.A., 1999. Combined mantle plume-island arc model for the formation of the 2.9 Ga Sumo-zero-Kenozero greenstone belt, SE Baltic shield: isotope and trace element constraints. Geochim. Cosmochim. Acta 63, 3579–3595.

Raase, P., Raith, M., Ackermand, D., Lal, R.K., 1986. Progressive metamorphism of mafic rocks from greenschist to granulite facies in the Dharwar craton of South India. J. Geol. 94, 261–282.

Radhakrishna, B.P., Sreenivasaiah, G., 1974. Bedded baryte from the Precambrian of Karnataka. J. Geol. Soc. India 15, 314–315.

Ramakrishnan, M., Venkatadasu, S.P., Kroner, A., 1994. Middle Archaean age of Sargur Group by single grain zircon dating and geochemical evidence for the clastic origin of metaquartzite from J.C. Pura Greenstone belt, Karnataka. J. Geol. Soc. India 44, 605–616.

Rollinson, H.R., Windley, B.F., Ramakrishnan, M., 1981. Contrasting high and intermediate pressures of metamorphism in the Archaean Sargur Schists of southern India. Contrib. Mineral. Petrol. 76, 420–429.

Seshadri, T.S., Chaudhuri, A., Harinadha Babu, P., Chayapathi, N., 1981. Chitradurga belt. In: J. Swaminath, M. Ramakrishnan (Eds.), Early Precambrian Supracrustals of Southern Karnatka. Geol. Surv. Ind. Mem. 112, 163–198.

Smithies, R.H., Champion, D.C., Cassidy, K.F., 2003. Formation of Earth's early Archaean continental crust. Precambrian Res. 127, 89–101.

Srikantia, S.V., Rao, M.S., 1990. Unusual concentric structure in komatiite of Kibbanahalli Arm of Chitradurga supracrustal belt near Banasandra, Karnataka. J. Geol. Soc. India 36, 424–429.

Srikantia, S.V., Venkataramana, P., 1989. The Archaean komatiites of Nagamangala supracrustal belt, Karnataka. J. Geol. Soc. India 33, 210–214.

Srikantia, S.V., Bose, S.S., 1985. Archaean Komatiites from Banasandra area of Kibbanahalli arm of Chitradurga Supracrustal belt in Karnataka. J. Geol. Soc. India 26, 407–417.

Stein, M., Hofmann, A.W., 1994. Mantle plumes and episodic crustal growth. Nature 372, 63–68.

Subba Rao, D.V., Naqvi, S.M., 1999. Archaean Komatiites from the older schist belt of Kalyadi in Western Dharwar Craton, Karnataka. J. Geol. Soc. India 53, 347–354.

Sun, S.-S., 1984. Geochemical characteristics of Archaean ultramafic and mafic volcanic rocks: implications for mantle composition and evolution. In: Kroner, A., Goodwin, A.M., Hanson, G.N. (Eds.), Archaean Geochemistry. Springer-Verlag, Berlin, pp. 25–46.

Sun, S.-S., Nesbitt, R.W., 1978. Petrogenesis of Archaean ultrabasic and basic volcanics: evidence from rare earth elements. Contrib. Mineral. Petrol. 65, 301–325.

Swaminath, J., Ramakrishnan, M., Viswanatha, M.N., 1976. Dharwar stratigraphic model and Karnataka craton evolution. Rec. Geol. Surv. India 107, 149–175.

Taylor, S.R., Gordon, M.P., 1977. Geochemical application of spark source mass spectrometry. III. Element sensitivity, precision and accuracy. Geochim. Cosmochim. Acta 41, 1375–1380.

Taylor, P.N., Chadwick, B., Moorbath, S., Ramakrishnan, M., Viswanatha, M.N., 1984. Petrography, Chemistry and isotopic ages of peninsular gneisses, Dharwar acid volcanic rocks and the Chitradurga granite with special reference to the late Archaean evolution of the Karnataka craton. Precambrian Res. 23, 349–375.

Taylor, S.R., McLennan, S.M., 1985. The Continental Crust: Its Composition and Evolution. Blackwell, Oxford, p. 312.

Venkata Dasu, S.P., Ramakrishnan, M., Mahabaleswar, B., 1991. Sargur–Dharwar relationship around the komatiite-rich J.C. Pura greenstone belt in Karnataka. J. Geol. Soc. India 38, 577–592.

Viljoen, M.J., Viljoen, R.P., Pearton, T.N., 1982. In: Arndt, N.T., Nisbet, E.G. (Eds.), The Nature and Distribution of Archaean Komatiite Volcanics in South Africa. Komatiites, Allen and Unwin, London, pp. 53–79.

Viswanatha, M.N., Ramakrishnan, M., Narayana Kutty, T.R., 1977. Possible spinifex texture in a serpentinite from Karnataka. J. Geol. Soc. India 18, 194–197.

Wilson, A.H., Carlson, R.W., 1989. A Sm–Nd and Pb isotope study of Archaean greenstone belts in the Southern Kaapvaal Craton, South Africa. Earth Planet. Sci. Lett. 96, 89–105.

Xie, Q., Kerrich, R., Fan, J., 1993. HFSE/REE fractionation recorded in three Komatiite-basalt sequences, Archaean Abitibi green stone belt: implication for multiple plume sources and depths. Geochim. Cosmochim. Acta 57, 4111–4118.

Zachariah, J.K., Hanson, G.N., Rajamani, V., 1995. Post crystallisation disturbance in the neodymium and lead isotope systems of metabasalts from the Ramagiri Schist belt, South India. Geochim. Cosmochim. Acta 59, 3189–3203.